# Hydrological impacts of climate change on rice cultivated riparian wetlands in the Upper Meghna River Basin (Bangladesh and India)

Mohammed M. Rahman [a,b,*], Julian R. Thompson [b], and Roger J. Flower [b]

[a] *Department of Irrigation and Water Management, Bangladesh Agricultural University, Mymensingh, Bangladesh*

[b] *Wetland Research Unit, Department of Geography, University College London, London WC1E 6BT, UK*

* Corresponding author: email mizaniwm@bau.edu.bd

Tel: +88 01717 825850; Fax: +88 091 61510

**Abstract** Riparian depressional wetlands (haors) in the Upper Meghna River Basin of Bangladesh are invaluable agricultural resources. They are completely flooded between June and November and planted with Boro rice when floodwater recedes in December. However, early harvest period (April/May) floods frequently damage ripening rice. A calibrated/validated Soil and Water Assessment Tool for riparian wetland (SWATrw) model is perturbed with bias free (using an improved quantile mapping approach) climate projections from 17 general circulation models (GCMs) for the period 2031–2050. Projected mean annual rainfall increases (200–500 mm per 7–10%). However, during the harvest period lower rainfall (21–75%) and higher evapotranspiration (1–8%) reduces river discharge (5–18%) and wetland inundation (inundation fraction declines of 0.005–0.14). Flooding risk for Boro rice consequently declines (rationalized flood risk reductions of 0.02–0.12). However, the loss of cultivable land (15.3%) to increases in permanent haor inundation represents a major threat to regional food security.

**Keywords** haor wetlands; Boro rice; floods; Bangladesh; climate change; SWAT

## 1 Introduction

The potential consequences of climate change on hydrological processes and associated sectors such as water resources, agriculture, aquatic ecology and human livelihoods have been extensively documented (e.g. Palmer *et al.* 2008, Dai *et al.* 2009, Strzepek *et al.* 2011, Tang and Lettenmaier 2012, Schneider *et al.* 2013, Brown *et al.* 2015). Currently 60% of global mean precipitation returns to the atmosphere as evapotranspiration (ET) and it has been suggested that this could increase to 80% by the end of the 21st century (Pan *et al.* 2015). Conversely,

Murray et al. (2012) showed that the world's 12 largest river basins would generate more runoff per unit of precipitation (i.e. higher runoff ratios) in a 2°C warmer world compared to a 1961–1990 baseline period. They attributed this to declines in both vegetation cover and transpiration due to soil water stress. Apportioning precipitation between ET and runoff relies upon the spatial characteristics of the landscape (land use, topography, geology), climatic variables and anthropogenic activities (Ponce 1989). Variability in the factors controlling runoff and, in turn, the complexity of their interactions, increases with spatial scale and likely accounts for contrasting results between these and other studies (Merz *et al.* 2011, Li *et al.* 2015). For example, whereas annual runoff sensitivity to temperature (change in runoff per unit change in temperature) is projected to be negative for arid regions, it is positive for the more humid catchments of southern Asia, where projected increases in intense monsoonal rainfall outpace increases in evapotranspiration (Arnell 2003, Tang and Lettenmaier 2012). Failing to adequately account for the influence of landscape and climate characteristics on hydrological processes may lead to misleading quantification of the impacts of climate change on regional/local water resources. For instance, extensive wetlands in a catchment can accelerate ET by the presence of open water and their limiting influence on soil water stress (Wu *et al.* 2016).

Many wetland environments, especially in less developed regions, represent key resources that provide vital ecosystem services for large human populations (Fox *et al.* 2011, Junk *et al.* 2013, Sun *et al.* 2017). Research is increasingly demonstrating the often detrimental consequences of climate change on wetlands (Acreman *et al.* 2009, Singh *et al.* 2010, Carolina and Jackson 2011, Greenberg *et al.* 2015, Thompson *et al.* 2016). For example, it has been suggested that North American Geographically Isolated Wetlands (GIWs) which are mainly sustained by precipitation and groundwater will experience shallower inundation that will extend for shorter periods due to increased water loss through accelerated ET (Johnson *et al.* 2010, Pitchford *et al.* 2012, Greenberg *et al.* 2015, Nungesser *et al.* 2015). Consequently, some wetland plant and animal species may be at risk of extinction (Pitchford *et al.* 2012, Greenberg *et al.* 2015, Nungesser *et al.* 2015). Furthermore, Carolina and Jackson (2011) showed that decreased precipitation might lower aquifer recharge in parts of Europe by up to 35% by the end of the 21st century. As a result, wetlands sustained by groundwater influxes will be less frequently hydraulically connected with the declining aquifers. However, in cases where connectivity between wetlands and the underlying aquifer is already relatively weak, as demonstrated for some prairie-pothole wetlands of North Dakota, USA

(Brooks *et al.* 2018), any impacts of climate change on groundwater may not be transmitted to the wetland's water budget.

In contrast to GIWs, hydrological responses of riparian wetlands to climate change are thought to be more complex and uncertain. This is because their hydrodynamics are strongly controlled by the flow characteristics of adjacent rivers and floodplains that themselves reflect hydrological conditions over their catchments (Mohamed and Savenije 2014, Popescu *et al.* 2015, Thompson *et al.* 2016). An altered climate might substantially shift river-wetland connectivity in terms of magnitude, timing, duration and frequency of water exchanges (Karim *et al.* 2015, 2016). For example, a study of the Sudd, South Sudan, demonstrated that changes in wetland inundation over the 20th century were strongly related to changes in climate some 1000 km upstream (Mohamed and Savenije 2014). Singh *et al.* (2010) showed that projected changes in runoff from the catchments draining to Loktak Lake, a Ramsar wetland in northeast India, dominated climate change-related modifications to water levels. At a much smaller scale, Thompson et al. (2017b) modelled declines in the occurrence and extent of floodplain inundation within a floodplain restoration site in eastern England which were driven by catchment-wide declines in precipitation and increases in evapotranspiration.

Wetlands across the world are being progressively exploited for a range of developmental purposes (Ramsar Convention on Wetlands, 2018). Asian wetlands are, for example, under immense pressure from agricultural conversion in order to satisfy the food demands of the region's growing population (McCartney *et al.* 2010, Gopal 2013, Junk *et al.* 2013, Molla *et al.* 2018, Quan *et al.* 2018). A case study of Tanguar haor, a Bangladeshi wetland listed as a Ramsar site of international importance, demonstrated rapid population growth in the region (240% over a decade) and a 112% increase in rice production (Sun *et al.* 2017). Enhanced productivity was largely attributed to wetland reclamation combined with increasing fertilizer application, irrigation and the use of hybrid varieties. In order to harness maximum wetland potentials, Nath and Lal (2017) even suggest a three-tier rice cultivation approach for different ecological zones (upper, mid shallow water and lower deep water) of such tropical wetlands. However, and as highlighted by Gopal (2013), climate change may have important impacts on wetlands throughout tropical and subtropical Asia with implications for their current and future use by human communities, including for agricultural cultivation.

The Upper Meghna River Basin (UMRB), which is shared by Bangladesh and India, contains hundreds of shallow depressional riparian wetlands that are locally known as haors (Fox *et al.* 2011, CEGIS 2012). These

wetlands are particularly concentrated in the downstream Bangladeshi part of the basin. Haor wetlands are extensively cultivated with Boro rice, a local high yielding variety. The region contains 16% of Bangladesh's 10.57 million ha of rice cultivating area and produces around 18% of the country's total rice production (CEGIS 2012). Rice is planted at the beginning of the dry season (December–March) when water levels decline following the seasonal flood period. Depending on the date of planting, the ripening period may span from April to May. However, the Boro rice harvest can be influenced by intense pre-monsoon rainfall during this period that results in rapid increases in river levels. This, in turn, can cause overbank flows that may inundate thousands of hectares of nearly ripened Boro rice within a matter of hours (Khan *et al.* 2005, CEGIS 2012, Khan *et al.* 2012).

In order to attain food security in the face of projected climate change (e.g. Dash *et al.* 2012, Chadwick *et al.* 2015, Li *et al.* 2016), better understanding of current and future hydrological regimes of the river-wetland system of the UMRB is urgently required. In particular, and given the large socio-economic implications of crop failures, it is important to assess whether a changing climate is likely to enhance or reduce flood risks within the basin's haor wetlands. Therefore, the objectives of this study are to: (i) build a catchment model capable of capturing the complex hydrology that includes interactions between rivers and wetland systems within the UMRB, (ii) project the response of haor hydrological regimes to climate change, and (iii) assess the impacts of these hydrological changes on the risks facing Boro rice cultivation within the basin's haor wetlands.


**2 Upper Meghna River Basin**

The Meghna River Basin is one of the three basins that constitute the world's sixth largest river system (1 629 470 km$^2$) containing the Ganges, Brahmaputra and Meghna rivers (Fig. 1(a)). The hydrological behaviour of the Meghna River Basin is generally characterized by the UMRB (63 746 km$^2$) that has its downstream outlet at Bhairab Bazar, approximately 50 km upstream of the confluence of the Padma (Ganges in India) and Meghna rivers (Rahman *et al.* 2016). Based on topographic and climatic characteristics (Fig. 1(b) and (c)), the UMRB can be divided into four sub-basins: (i) the Barak River Basin, (ii) the Meghalaya Basin, (iii) the Tripura Basin and (iv) the Sylhet Basin. The latter is dominated by extensive floodplains and about 370 haor wetlands with a combined area of 8573 km$^2$, or 42% of the total area of the Sylhet Basin when completely inundated (CEGIS, 2012, Islam, 2010).

Elevation of the UMRB ranges from less than 5 m below mean sea level (m.s.l.) at the centre of the Sylhet Basin to around 3000 m above m.s.l. in the Lushai Hills where the Barak River originates (Fig. 1(b)). The major land cover classes, derived by reclassifying Global Land Cover (GLC) data (Hansen *et al.* 2000) using Google Earth[TM] imagery and the first author's knowledge of the basin, are deciduous forest (30%), evergreen forest (29%), rice (29%) and tea/shrub (11%). A very small proportion (1%) is classed as non-vegetation (i.e. water and urban). The three Indian upland basins (Meghalaya, Tripura and Barak) are mainly covered by forest, whereas land use in the Sylhet Basin is dominated by rice cultivation. The hydrological year (April–March) is divided into four seasons: pre-monsoon (April–May), monsoon (June–September), post-monsoon (October–November) and the dry season (December–March). Annual rainfall ranges from 1300 mm over the Lushai Hills to over 8300 mm in the northwest (Fig. 1(c)). The basin includes the world's rainiest places: Cherrapunji (approx. 11 430 mm year^{-1}) and Mawsynram (approx. 11 873 mm year^{-1}).

*Figure 1*

The Surma and Kushiyara rivers, the two major rivers of the basin, originate after the bifurcation of the Barak River at Amalshid and reunite at Bajitpur to form the Meghna River (Fig. 1(a)). Drainage patterns are complex in the lower Sylhet Basin and include the numerous haor wetlands. The deepest portions of the haors, locally called beels, seldom completely dry out and water levels are maintained by exchange with shallow aquifers (Rahman *et al.* 2016). Beels are an important habitat in the dry season for hundreds of fish species and are managed as fisheries by local communities (Miah *et al.* 2017). They also provide a source of irrigation water for Boro rice (Hasan and Hossain 2013). Almost all haors are traversed by or connected to rivers so that river–wetland interactions exert important controls on hydrological regimes. River flow and water levels are highly seasonal in response to the Asian monsoon. As river levels rise with the rains, haors become hydraulically connected to rivers that provide large influxes of water. Peak haor water levels normally occur between June and October. Subsequently, as river flows decline following the monsoon, water drains back towards the rivers (Rahman *et al.* 2016). Further declines in water levels between December and January are driven by evaporation and seepage. At this time, the shallow haor wetlands turn into extensive arable land for Boro rice cultivation. Although dry-season Boro rice is the main crop, Aman rice, another local rice variety, is cultivated on comparatively higher-elevation land that is less prone to inundation during the period August–December (Sarker *et al.* 2017).

# 3    Methods

## 3.1 Development of a catchment model of the UMRB

This study employs a modified version of the Soil and Water Assessment Tool (SWAT) hydrological model. With its numerous derivatives (Liu *et al.* 2008, Wang *et al.*, 2008), SWAT is a conceptual, semi-distributed and process-based catchment model. It is probably the most widely used catchment modelling platform and has been employed extensively for assessing the hydrological impacts of climate change (e.g. Shrestha *et al.* 2012, Khoi and Suetsugi 2014, Neupane and Kumar 2015). The SWATrw model (SWAT for riparian wetland) is an enhanced version of SWAT (rev. 627) which replaces the original unidirectional hydrological interactions between rivers, aquifers and riparian wetlands such as haors with more robust bidirectional approaches based on hydraulic principles (Rahman *et al.* 2016). All other process representations are identical to those within SWAT.

During catchment delineation (carried out using ArcSWAT, a GIS interface for SWAT), a river basin is discretized into sub-basins based on the topography and river network (Neitsch *et al.*, 2011). A sub-basin is further discretized into hydrological response units (HRU) each having unique combinations of surface slope, land use and soil. Although a sub-basin area is apportioned among its constituent HRUs, these HRUs do not have any spatial address within the sub-basin. The data employed in this discretization for the UMRB model, as well as the meteorological data used to drive the model and river flow data employed for calibration/validation, are summarized in Table 1. The automatic delineation algorithm reproduced the river network and associated sub-basins reasonably well for the three upper Indian sub-basins (Meghalaya, Barak River and Tripura). However, digital elevation model (DEM)-based network delineation failed to reproduce the complex drainage network of the flat Sylhet Basin, an issue reported elsewhere in similar situations (Poggio and Soille 2011). Rivers and their courses in these flat deltaic areas are also controlled by hydro-sedimentary dynamics and human interventions (e.g. river diversion for irrigation) whilst the presence of depressional haors traversed by many small rivers complicates automatic network delineation. Therefore, the river network within the Sylhet Basin was first manually digitized using multi-source data comprising polyline features provided by the Center for Environmental and Geographic Information Services (CEGIS), Bangladesh, satellite-derived imagery (Google Earth[TM] and ESRI) and published documents (Khan *et al.* 2005, Baki *et al.* 2008). The network derived in this way was used within the 'Burn In' function of the automatic delineation algorithm to generate the drainage boundary (i.e. sub-basin) of each river. The UMRB model comprised 267 sub-basins and 1237 HRUs (see Supplementary material, Fig. S1).

*Table 1*

Wetlands within SWATrw are considered as depressional water bodies that can interact with nearby rivers and underlying aquifers. SWATrw (in common with the simpler wetland representation in SWAT) is currently restricted to the simulation of one wetland within an individual sub-basin. Thus, multiple wetlands in a sub-basin are aggregated into a Hydrologic Equivalent Wetland (HEW) by combining their hydrological attributes (water surface area and volume). This HEW approach has been successfully employed for the modelling of American prairie wetlands using SWAT (Wang *et al.* 2008). The SWATrw model adopts a robust and flexible volume–area–depth relationship to model the geometry of a sub-basin level wetland (Hayashi and van der Kamp 2000):

$$A_{\text{wet}} = b \left( \frac{D_{\text{wet}}}{D_{\text{wet},0}} \right)^{2/p} \tag{1}$$

$$S_{\text{wet}} = \left( \frac{b}{1 + \frac{2}{p}} \right) \times \frac{D_{\text{wet}}^{\left(1 + \frac{2}{p}\right)}}{D_{\text{wet},0}^{\frac{2}{p}}} \tag{2}$$

where $S_{\text{wet}}$ and $A_{\text{wet}}$ denote wetland water volume and surface area, respectively, at depth $D_{\text{wet}}$; $b$ and $p$ are the scale and shape parameters of the wetland, respectively; and $D_{\text{wet},0}$ indicates unit wetland depth. The parameters for a particular wetland can be calibrated against the observed area-depth relationship curve outside of SWATrw (e.g. using a spreadsheet programme). However, this approach is often limited by the scarcity of observed, and sufficiently detailed, wetland hypsographic data as in the case for the UMRB. This issue can be overcome by calibrating against time series of known hydrological quantities (e.g. discharge at the wetland / sub-basin outlet) simulated by a catchment model (Wang *et al.* 2008, Feng *et al.* 2013). This is premised upon the assumption that, where wetlands exert a considerable influence on catchment hydrology, justifiable simulation performance is not achievable until the wetlands are properly represented.

Spatial data describing the maximum inundated area of haor wetlands were collected from CEGIS (see Fig. 1(a)). The maximum wetland water surface areas of all wetlands within a sub-basin were summed to provide a sub-basin level total. The corresponding wetland depth was retrieved from Google Earth^TM by manually searching for the highest and lowest elevations within the extent of wetlands in each sub-basin. Through the specification of the water surface area and depth at maximum capacity, properly calibrated shape ($p$) and scale ($b$) parameters that define a wetland's geometry are expected to produce a reasonable HEW for the associated sub-basin (see Rahman *et al.* 2016 for details).

A distinguishing feature of SWATrw over SWAT is that a wetland is allowed to receive water from rivers and underlying aquifers as well as contributing water to rivers and aquifers based on hydraulic principles. Such capability is essential for the accurate modelling of wetlands, such as the haors of the UMRB, which display strong, bidirectional exchanges with other surface waters and groundwater. The approaches used to represent these processes are detailed by Rahman *et al.* (2016) (and summarized in the Supplementary Material, Fig. S2).

Rice cultivation is the major dry season land use in the haor dominated Sylhet Basin. Therefore, information regarding cultivation practices (e.g. planting, irrigation, fertilization) was provided in the model according to the methods generally followed in the area (CEGIS 2012). Estimation of ET, particularly in the Sylhet Basin, where dry season rice cultivation is transformed into inundated areas in the wet season, is critical to realistic hydrological simulations. In the absence of pre-calculated potential ET (PET) time series, SWATrw (and SWAT) can estimate PET using one of three methods: Priestley-Taylor (P-T), Penman-Monteith (P-M) and Hargreaves (Har). The PET is converted to actual ET (AET) by taking into account crop and soil resistances to water movement. In the case of wetlands, PET is multiplied by a calibration term, WETEVCOEFF, in order to provide AET. The SWATrw model uses the simulated extent of inundation within each haor to determine the relative extent of ET from wetland surfaces and from dry land that, according to the specified cultivation practices, may be rice or bare soil. During calibration (described below), application of the more physics-based P-M method provided superior reproduction of observed river discharges. The P-M method was therefore used in both the baseline and climate change scenarios simulated using the SWATrw model.

The UMRB SWATrw model was run at a daily time step. For the data-scarce UMRB, the meteorological data used to drive the model were compiled from multiple sources (Fig. 1(a) and

Table ). This was a particular issue for the Indian part of the basin for which IMDgrid and IMDdist rainfall data were used for the calibration and validation periods (see below), respectively. Given the daily time step of the model, monthly IMDdist rainfall and CRU temperature data (used for the whole basin) were disaggregated to a daily resolution using the stochastic Monthly to Daily Weather Converter (MODAWEC) developed by Liu *et al.* (2009). This distributes monthly total rainfall among the given wet days in a month. The latter were retrieved from the CRU database. Similarly, daily temperature (maximum and minimum) was generated based on the standard deviation of temperature for a specific month in a year. The suggested default equations were used to calculate the required standard deviations of temperature for each month (see Liu *et al.* 2009). Daily observed time series of humidity, wind speed and solar radiation were unavailable. Therefore, the built-in weather generator of SWAT, WXGEN (Sharpley and Williams 1990), was used to produce these climate data using monthly climate statistics (mean, standard deviation, number of wet days) estimated from CRU and FAO CLIMWAT 2.0 databases that include records for 12 stations within the UMRB. In data-scarce regions, such an approach is generally used to overcome limitations imposed by limited availability of daily weather data (e.g. Fadil *et al.* 2011, Lee *et al.* 2018).

The model was manually calibrated by comparing observed and simulated mean monthly discharges at 15 river gauging stations (Fig. 1(a)) for the period 1990–2003 followed by validation using the period 2004–2010. Selection of these periods was determined by the availability of both the meteorological data used to drive the model and discharge records for calibration / validation. In order to reduce uncertainties associated with initial conditions, the model was additionally run for the three preceding years (warm-up period) before the calibration and validation periods. Alongside graphical comparisons, model performance was statistically evaluated using the statistical indicators recommended by Moriasi *et al.* (2007): Nash-Sutcliffe efficiency (NSE) (Nash and Sutcliffe 1970), percent bias (PBIAS) (ASCE 1993, Moriasi *et al.* 2007), ratio of root mean square error to the standard deviation of observed data (RSR) (Moriasi *et al.* 2007), and the coefficient of determination ($R^2$). Table 2 summarizes the parameters varied during calibration and their final values. During initial calibration runs, it was observed that simulated flows were most sensitive to these parameters justifying their selection.

*Table 2*

*3.2 Simulation of climate change*

Most assessments of the hydrological impacts of climate change employ projections of future climate from global climate models or general circulation models (GCMs). Since existing GCMs are not structurally unique, their simulated climate outputs may have considerable disagreements with corresponding historical observed meteorological data (Chang and Jung 2010, Lutz *et al.* 2016). To account for this GCM-related uncertainty, many studies use ensembles of GCMs rather than relying on a single GCM (Carolina and Jackson 2011, Velázquez *et al.* 2013, Tang *et al.* 2016). In this study 17 GCMs from Phase 5 of the Coupled Model Intercomparison Project (CMIP5) were selected (Table ). Their respective daily time series of historical baseline (1981–2000) and future (2031–2050) climate data (precipitation and temperature) were acquired from the NASA Earth Exchange Global Daily Downscaled Projections (NEX-GDDP) repository[1]. The NEX-GDDP database is one of a few initiatives to downscale CMIP5 GCM data to finer spatial resolution (~27 km or ~0.25°) for the entire world and to make them freely available for use in scientific research. The 2031–2050 period was selected since Bangladesh has aspirations to be a developed nation by 2041 (Jha 2017) and its development plans up to and beyond this date include haor agriculture for which there is a need to incorporate the potential impact of climate change. For future projections, the representative concentration pathway RCP4.5 scenario, associated with the stabilization of radiative forcing at 4.5 W m$^{-2}$ at the end of the 21st century, was selected. World-wide policy makers and climate modellers have recognized this as the most optimistic scenario if plans to combat the current greenhouse gas emission rates are to be properly implemented (IPCC 2013, UNFCCC 2015). RCP4.5 has been employed in a number of catchment / wetland specific climate change impact studies (e.g. Yan *et al.* 2015, Thompson *et al.* 2017a, Hudson and Thompson 2019) employing similar approaches. Therefore, this study expands the geographical range of these assessments.

*Table 3*

A comparison of the NEX-GDDP climate data (or raw GCM data) for the 1981–2000 baseline period with the corresponding observed data available within the study area was initially undertaken. Considerable bias in the raw GCM data was evident. NEX-GDDP mean annual rainfall anomalies (deviation from the observed values) across the UMRB varied between 3150 mm year$^{-1}$ (under-prediction) and 1400 mm year$^{-1}$ (over-prediction) (see

---

[1] https://nex.nasa.gov/nex/projects/1356/

Supplementary material, Fig. S3(b)–(r)). The spatial pattern of these anomalies was very similar for all GCMs and included under-prediction of rainfall in the wettest areas around Cherrapunji in the northwest. Conversely, most GCMs over-predicted rainfall in the drier Tripura, Barak River and southern Sylhet sub-basins. Biases in the NEX-GDDP data may be linked to the reference data used for bias correction. NEX-GDDP uses globally available gridded reference climate data derived from either remotely sensed information (e.g. Tropical Rainfall Measuring Mission, TRMM; Global Precipitation Climatology Project, GPCP) or available meteorological stations (e.g. NCEP-NCAR reanalysis, CRU TS2.0). Previous studies have found that most of these data are unable to capture the variability and magnitude (with most under-estimating) of orographic rainfall in the UMRB region (Immerzeel 2008, Nishat and Rahman 2009, Moffitt *et al.* 2011, Rahman *et al.* 2012). Therefore, further bias correction of the NEX-GDDP data using reliable and representative ground-based observations from the relatively dense meteorological station network was undertaken.

The quantile mapping (QM) method which was applied overcomes the limitations of the widely used delta change method wherein bias-corrected values derived from raw GCM data for a reference period can only conserve the mean of the corresponding observed data but not the variance (Ines and Hansen 2006, Leander and Buishand 2007, Hwang and Graham 2014). In principle, any statistical bias correction method first establishes a relationship between observed and raw GCM data for a reference (or baseline) period (respectively denoted as Obs-ref and raw-GCM-ref). Assuming this relationship will persist in the future, it is used to remove biases in future raw GCM data (raw-GCM-fur). The QM approach developed for this study can be described with five sequential steps: (i) discretizing the area of interest (here the UMRB) into homogeneous climate zones (HCZ), (ii) producing representative observed and modelled (raw GCM) time series of climate variables for each HCZ, (iii) clustering the time series into 12 calendar months, (iv) constructing cumulative distribution functions (cdf) for the monthly clustered observed and modelled values, and (v) estimating biases or correction factors (CF) at specific quantiles for raw-GCM-ref data and, finally, using these correction factors to adjust the biases in the raw-GCM-fur data. These steps are illustrated in Fig. 2. Since biases in raw-GCM-ref data are estimated with respect to Obs-ref data, first the area represented by each meteorological station (HCZ) is identified. However, the approach used herein differs from commonly used practices where a HCZ is a large GCM grid (~250 km × 250 km) that may contain several meteorological stations. Since the NEX-GDDP raw GCM data are already spatially downscaled to a finer grid with 88 grid cells covering the UMRB compared to the 26 meteorological stations, the opposite

approach was followed. This is particularly advantageous for the SWATrw model where data from a meteorological station can be applied to several sub-basins depending on their proximity to the station. Since increasing extreme events in climate variables (especially rainfall) cannot often be well fitted to a theoretical probability distribution, the empirical cdf (ecdf) approach was used as practised elsewhere (Hwang and Graham 2014, Rashid *et al.* 2015). Therefore, any reference to cdf hereafter refers to ecdf unless otherwise stated. In principle, the cdf of bias-free raw-GCM-ref data should perfectly match the corresponding observed cdf. Later the signed CFs obtained for the reference period were used as additive factors to correct future raw GCM data.

*Figure 2*

The final step of the QM method is graphically illustrated in Fig. 3 by generating, for the sake of simplicity, the necessary curves from a theoretical cdf (e.g. a normal distribution) rather than an ecdf. One notable limitation of existing QM methods (Ashfaq *et al.* 2010, Themeßl *et al.* 2012, Hwang and Graham 2013) is their inability to adjust the frequency of dry days because a common cdf value between the Obs-ref and raw-GCM-ref curves at their lowest points (i.e. dry days) is rarely found (Sulis *et al.* 2012, Rashid *et al.* 2015). This study addressed this issue by considering two conditions: underestimated (Fig. 3(a)) and overestimated (Fig. 3(b)) dry days in the raw-GCM-ref data. Procedurally, the value of the cumulative probability density (cpd) or cdf corresponding to a rainfall amount in a wet day of the raw-GCM-ref data is first determined (A in Fig. 3). Then, B is the corresponding point on the observed cdf curve (Obs-ref) leading to a negative (Fig. 3(a)) or positive (Fig. 3(b)) bias of AB relative to raw-GCM-ref rainfall (A). The aforementioned strategy of correcting wet days is valid for any cdf value greater than the lowest common cdf (lccdf) value between Obs-ref and raw-GCM-ref (E in Fig. 3):

$$\text{lccdf} = \max\left(\text{cdf}_{\text{Obs}-\text{ref},0}, \text{cdf}_{\text{raw}-\text{GCM}-\text{ref},0}\right) \qquad (3)$$

where $\text{cdf}_{\text{Obs}-\text{ref},0}$ is the cdf value of the observed climate variable (rainfall in the example) corresponding to the lowest value (zero rainfall in the example) and $\text{cdf}_{\text{raw}-\text{GCM}-\text{ref},0}$ has the same meaning as $\text{cdf}_{\text{Obs}-\text{ref},0}$ but for raw-GCM-ref data. The next step is to adjust the dry days in the raw-GCM-ref data. In the case of underestimated dry days (Fig. 3(a)), any raw rainfall equal to or less than the threshold value (*F*) corresponding to the lccdf is converted to dry days in order to match the number of dry days in the Obs-ref data. To adjust overestimated dry days (Fig. 3(b)), the dry day error fraction is estimated as follows:

$$\text{ddef} = (\text{cdf}_{\text{Obs-ref,0}} - \text{lccdf})/\text{lccdf} \qquad (4)$$

where ddef is the dry day error fraction. The absolute value of ddef is an estimate of what percentage of dry days in the raw-GCM-ref data is to be converted to wet days. The rainfall range of those wet days lies between above zero and a threshold corresponding to the lccdf of Obs-ref data (F in Fig. 3(b)). While adjusting these dry days in the time series of raw-GCM-ref data, a random value from the space between zero and the threshold rainfall is generated from a pre-defined distribution. This distribution assumes that the probability of a random value being '0' is $[1 - \text{abs}(\text{ddef})]$, and for all non-zero values (i.e. wet days) within the threshold, the probability is identical i.e. uniform distribution.

*Figure 3*

In order to correct the future raw GCM data (i.e. raw-GCM-fur), the dry day frequency is first fixed. Assuming the mismatch in the dry day frequency of raw-GCM-ref data as represented by ddef will persist in the future, the dry day cdf value of raw-GCM-fur data is adjusted accordingly. To do so, the dry day frequency of raw-GCM-fur data is either increased or reduced to the corrected value (J in Fig. 3) by respectively adding or subtracting the product of ddef and the future raw CDF value at zero rainfall (i.e. $\text{cdf}_{\text{raw-GCM-fur,0}}$). Subsequently any raw-GCM-fur values greater than the lccdf among Obs-ref, raw-GCM-ref and cor-GCM-fur (see Equation (5)) are adjusted by adding the previously estimated signed CF corresponding to the cdf of the raw-GCM-fur value. In Fig. 3, for example, the lccdf is still at E, since J (i.e. corrected dry day cdf in the future GCM data) is below E. The remaining uncorrected raw-GCM-fur values lying at or below the lccdf are corrected by randomly choosing a value from the data space JH having a distribution such that the probability of a value being zero (i.e. dry day) is $[1 - \text{abs}(\text{ddef})]$. Here, ddef is estimated as follows:

$$\text{lccdf} = \max(\text{cdf}_{\text{Obs-ref,0}}, \text{cdf}_{\text{raw-GCM-ref,0}}, \text{cdf}_{\text{cor-GCM-fur,0}}) \qquad (5)$$

$$\text{ddef} = (\text{cdf}_{\text{cor-GCM-fur,0}} - \text{lccdf})/\text{lccdf} \qquad (6)$$

The same procedure was applied to correct raw temperature data with the exception that the dry day frequency for a calendar month is instead the coldest day frequency.

The calibrated SWATrw model was driven with the climate time series data (rainfall and temperature) for the baseline (1981–2000) and future (2031–2050) periods. The remaining climate data (wind speed, humidity and solar radiation) required by the SWATrw model for the calculation of P-M PET were assumed to be same as for

the baseline, since future projections were not available. In humid environments, where precipitation predominantly controls the outflows of a catchment, perturbing a model with only precipitation and temperature is considered appropriate, as demonstrated by Ouyang *et al.* (2015) for a Chinese catchment, although inclusion of other climatic variables can increase projection confidence. It is appropriate to note that the NEX-GDDP climate data for the historical period were only available up to 2005, whereas the training period (calibration and validation) of the SWATrw model was, as described above, 1990–2010. Therefore, the first 45% of the baseline period (i.e. 1981–1989) falls outside the training period. In an ideal situation, the baseline period should be within a period for which model parameters are evaluated against some statistical criteria (Thompson *et al.* 2014, 2016, Zhu *et al.* 2016). Since this overlapping of training and baseline periods is conditioned by the availability of data, it is not always possible, as in the present study, to conform to the ideal practice.

## 4    Results and discussion

### *4.1 Performance of the calibrated SWATrw model for the UMRB*

The performance of the SWATrw model in simulating monthly mean discharge for both the calibration and validation periods is acceptable (at least 'satisfactory' and in many cases 'good' or 'very good') at nine of the 15 gauging stations (Table , Figs 4 and 5; see Supplementary material, Fig. S1 for station names and their catchments). Performance at the remaining six stations is less satisfactory for at least part of the training period (i.e. the calibration and/or validation periods). At three gauging stations in the Meghalayan sub-basins (Sarighat, Islampur and JariaJanjail) performance is acceptable for the calibration period but is poorer for the later validation period. This may be linked to inconsistencies between the IMDgrid and IMDdist rainfall data that are used for the calibration and validation periods, respectively. For instance, mean annual rainfall over the Sarighat sub-basin was 5283 mm for the calibration period compared to 4166 mm for the validation period. Such large disparities were not evident in locations where rainfall data from a consistent source (i.e. BMD) were available. These differences are likely to be responsible for the underestimated discharge in the validation period (PBIAS = 51.22%). The commonly used split sample test (SST), in which single sourced time series of climatic data are split between calibration and validation periods, could not be employed in this study due to limited data availability. Hydrological model performance usually declines for periods that are climatically contrasting to the calibration

14

period. Deterioration in performance is more severe when a model calibrated under wetter conditions is applied to a drier period compared to the opposite situation (Seibert 2003, Coron *et al.* 2012). This could account, at least partially, for the poorer validation performance for the Sarighat sub-basin. Simulated discharges for the Kamalganj and Saistaganj stations (Fig. 5(d) and (e)) reveal that the model overestimates peak and recession flows of the annual hydrographs. There is a barrage regulating flows from the upper 36% of the Saistaganj sub-basin. However, information on its physical structure and operation were not available, preventing its inclusion within the model. This might potentially degrade the model performance for this sub-basin.

*Figure 4, Figure 5*

The Bhairab Bazar gauging station on the Meghna River is the outlet of the UMRB (Fig. 1(a)). Model performance is satisfactory (S) and unsatisfactory (US) for the calibration and validation periods, respectively (Table ). The model tends to underestimate observed discharge (Fig. 5(g)), leading to positive PBIAS values (Table ). Monsoonal peak flows are often underestimated (e.g. in 1990–1994, 2001 and 2005–2006), while discharges during the recession of the annual hydrographs starting in the late monsoon are consistently underestimated. In the dry season (December–March), the Meghna River is simulated as completely drying out, while the available records for 1998 and 2006 indicate discharge values during this period of between 1600 and 3864 $m^3 s^{-1}$. To investigate this limitation, daily discharges of the Meghna River at Bhairab were simultaneously compared with those from three large catchments further upstream, the Barak, Meghalaya and Tripura (see Fig. 1(a) for locations). Of these three catchments, runoff generated from the wettest catchment – Meghalaya – predominantly shapes the hydrograph of the basin outflows at Bhairab (see Supplementary material, Fig. S4). Therefore, unrealistic simulation of the Meghalaya catchment would greatly influence model performance at the basin outlet. While calibrating the Meghalayan Laurergahr catchment (2493 $km^2$), on average around 790 mm of shallow aquifer water had to be withdrawn from the catchment's hydrological processes by transferring it to the deep aquifer system (higher RCHRG_DP value). It is suspected that the aquifer in the Laurergahr catchment is not absolutely confined within the catchment boundary (as assumed within the model set up). Instead, it may connect with aquifers and surface water bodies (rivers and wetlands) in the downstream Sylhet catchment. Therefore, water that is removed from the upstream Laurergahr catchment may appear in the hydrological system further downstream, a process that could not be represented within the model. Had such large volumes of water (790 mm

$\times$ 2493 km$^2$) not been removed from the flows originating in the upper catchment, outflows (surface and/or baseflow) from the UMRB would have significantly increased.

This zero boundary flow assumption between sub-basin aquifers in SWATrw (also in SWAT) may be even more unrealistic for shallow sloping plain areas such as the lower Sylhet catchment of the UMRB. In order to preserve the high density of river networks in the Sylhet catchment, as many sub-basins as the number of rivers were manually delineated. However, the number of sub-basins would have been reduced if some small sub-basins were amalgamated with their neighbours to form larger sub-basins. This would, however, necessarily simplify the river network. The assumed isolated aquifers (zero boundary flow) underlying each of the sub-basins are unlikely to accurately represent the continuous shallow aquifer that extends across the plains of the flat Sylhet catchment. In such situations, the incorporation of a more robust physics-based distributed groundwater model would be more appropriate although this is not possible in the current version of SWATrw / SWAT.

Another possible reason for underestimation of discharge at Bhairab may be associated with the BWDB rating curve for this station. Uncertainties in rating curve generated flows may be induced due to altered channel geometry, unsteady flow, changing channel roughness (for example due to vegetation growth) and backwater effects (Di Baldassarre and Montanari 2009, Hidayat *et al.* 2011). While details regarding the frequency with which the rating curve at this site is updated are not available, it has been reported that the flow regime of the Meghna River at Bhairab is influenced by backwater from the downstream confluence with the Padma River at Chandpur (Chowdhury and Salehin 1997, Chowdhury and Ward 2004). As a result, the BWDB rating curve might overestimate discharges due to backwater induced higher river stages. This could, at least in part, account for some differences between observed and simulated outflows from the UMRB.

Alam (2011) found that a geomorphological based hydrological model (GBHM) of the Meghna River Basin overestimated monsoonal flows at the Bhairab Bazar outlet, whereas post-monsoonal recession flows were consistently underestimated. Although the former discrepancy was attributed to the overestimation of overland flows and higher TRMM rainfall, a clear reason for underestimated recession flows was not evident. In another study using the macroscale conceptual H08 hydrological model (Hanasaki *et al.* 2008), simulated monsoonal peak flows at the basin outlet were underestimated (Masood *et al.* 2015). Moreover, a larger contribution of subsurface

flow (69%) to total outflow was simulated supporting our assertion that the SWATrw model may not adequately propagate groundwater flow to downstream parts of the UMRB.

## 4.2 Projected future climate of the UMRB

Before discussing the projected future climate of the UMRB, evidence is provided to demonstrate how the QM bias-correction approach improves the raw GCM data. This is done using results for one GCM, CCSM4, and one meteorological station as an example. For the two situations shown in Fig. 3 (over- and under-predicted dry days), daily rainfall data for August and November are illustrated in Fig. 6(a) and (b), respectively; and the corresponding temperature data for August are shown in Fig. 6(c). Unlike the over- or under-predicted dry day frequency for rainfall, the frequency of lowest temperature was found to be unique (close to zero in the present study) for all temperature data sets, thereby eliminating the necessity of frequency adjustment. It is evident that unlike temperature, daily rainfall does not follow a typical normal distribution. The QM method fits the raw-GCM-ref rainfall to the observed rainfall during the reference period. In particular, both overestimated (inset in Fig. 6(a)) and underestimated (inset in Fig. 6(b)) dry days in the raw-GCM-ref data are exactly matched to the respective observed cdf points corresponding to zero rainfall. Moreover, change in dry day frequency between the reference and future period in the raw GCM data is maintained in the corrected GCM data. For example, in the inset of Fig. 6(a), the raw rainfall data (raw-GCM-ref and raw-GCM-fur) indicate more dry days in the future compared to the reference period (difference of dry day cdf $= 0.255 - 0.224 = 0.031$). Since the QM approach takes this trend into account while correcting the raw rainfall data, the trend appears in the corrected rainfall data (cor-GCM-ref). This ability of the QM approach is also clearly seen in the case of under-predicting dry days (Fig. 6(b)).

*Figure 6*

Rather than showing projections from individual GCMs, Fig.7 provides the ensemble statistics (mean, CV and change with respect to the baseline) of the rainfall projections from the 17 GCMs. Compared to the baseline, projected mean annual rainfall increases across the basin by between 200 and 500 mm (10 and 7%) with the largest increases projected for the wettest region, Cherrapunji. Variations between the different GCMs (i.e. CV) are no more than 10% across most of the basin, although they are higher (20%) around Cherrapunji. These annual

17

changes are strongly controlled by the projected increases in rainfall during the monsoonal months (June–September). Pre-monsoonal (April and May) rainfall is projected to decline (by between 25 and 75 mm (21–22%)) across the basin by all GCMs. As a result, the flash floods that characterize baseline conditions may decline due to a reduction in the frequency and/or magnitude of intense pre-monsoonal rainfall events. The dry season (December–March) is projected to become slightly wetter, e.g. 5–25 mm (8–18%) for March. There are relatively large variations between different GCMs for November–February (CV: 30–90%) with both increases and decreases being projected.

*Figure 7*

Using daily rainfall time series (1984–2016), Basher *et al.* (2018) found that pre-monsoonal and monsoonal wetness over the haor region of Bangladesh have reduced, as evidenced by a number of extreme rainfall indices. After first identifying the MRI-AGCM3.2S GCM as a good simulator of the Asian monsoon, Masood and Takeuchi (2016) showed that, compared to a 1979–2003 baseline period, annual maximum rainfall within the Meghna River Basin could increase by 23% under the A1B climate scenario for the 2015–2039 period. This increase is considerably larger than those identified in the current study (10%). A primary reason for these differences is most probably the use of different climate change scenarios. The present study employs the RCP4.5 scenario, whereas Masood and Takeuchi (2016) used the A1B emissions scenario which is associuated with an atmospheric $CO_2$ concentration that lies between those of RCP6 and RCP8.5 (Meinshausen *et al.*, 2011). Future development of the current study could extend the simulations to these more extreme climate scenarios.

Inter-GCM and spatial variations in the projected changes in temperature are relatively small compared to those for precipitation. A consistent increase in mean monthly temperature compared to the baseline is projected at all 10 meteorological stations (Fig. 8). The magnitude of these changes ranges from 1.13 to 1.68°C (Fig. 8a). The dry season months see not only the largest increases in temperature but also greater spatial variability.

*Figure 8*

### 4.3 Projected changes in river discharge

In order to investigate the impacts of projected climate change on river discharge within the UMRB, the basin is divided into six regional/major sub-basins defined by selected gauging stations (Fig. 9). The Meghalaya catchment was divided into three sub-basins so as to better investigate the hydrological responses to its highly spatially

variable rainfall. For a sub-basin with more than one outlet (e.g. the Barak River), the combined flows of these outlets represent the total outflow of the sub-basin.

*Figure 9*

Figure 10 shows the mean monthly discharge for the baseline and box-and-whisker plots derived from the 17 GCMs for each of the major sub-basins. It demonstrates only very small absolute changes in mean monthly discharge between the baseline and projected ensemble mean during the dry season months of December–March for all of the sub-basins. The outlet of the basin, Bhairab Bazar at the downstream end of the Sylhet sub-basin, experiences small increases in dry season discharges for the ensemble mean. The largest increase ($107 \text{ m}^3 \text{ s}^{-1}$ / 54%) is projected for March and largely originates from increases in the Barak (60%) and Meghalaya (25%) sub-basins. Increasing outflows from the UMRB in December and January are largely the result of upstream increases from the West Meghalaya although inter-GCM uncertainty is relatively large compared to the other sub-basins.

*Figure 10*

Decreasing mean projected discharge of between 5 and 18% in April and May for all major sub-basins except the West Meghalaya may yield some positive impacts for the current flash flooding problems within the haor areas during the Boro rice harvesting periods. Conversely, increases in discharge during the monsoon months (June–September) are projected for all sub-basins. The largest absolute and percentage increases are $2420 \text{ m}^3 \text{ s}^{-1}$ (Bhairab) and 31% (Barak River), respectively. The greatest inter-GCM variability in projected discharges is for the early part of the monsoon period (June and July).

Long-term mean discharges, such as those presented in Fig. 10, can only be relied upon in decision-making regarding water resources management if all constituting values concentrate towards the mean value, thus showing low temporal variation. Therefore, the temporal variation of mean monthly discharge was investigated through the derivation of the CV for each month at each sub-basin outlet (see Supplementary material, Fig. S5). Under the baseline period and throughout the UMRB, low flows in the dry and pre-monsoon seasons show larger temporal variations (CV: 50–400%) compared to the high flows of the monsoon and post-monsoon seasons. This pattern is retained in the future projected discharges, but with larger temporal variation relative to the baseline for all calendar months except December–February.

The GLC land-use data used in the SWATrw model represents the average land use during the period 1981–1994. It was assumed that land use was unchanged throughout both the baseline and future periods. Recent studies

19

have suggested that hillslope areas of the basin are being increasingly modified through clearing of natural vegetation for pineapple and rubber cultivation, as well as human settlements (RRCAP 2001, Sherwood 2009, Thompson and Balasinorwala, 2010). These changes may alter the rainfall–runoff characteristics, with implications for downstream river discharge and flood extent (Hurkmans *et al.* 2009, Yan *et al.* 2013). A further extension of the current research could, therefore, employ a range of alternative future land cover distributions, informed by remote-sensing based analysis of recent changes, to investigate their potential impacts on the hydrology of the UMRB and its haor wetlands. This could be done both in isolation and in combination with the climate change projections employed in the current study.

### *4.4 Projected changes in wetland inundation*

Patterns in the spatial and temporal extent of inundation of haor wetlands are of enormous socio-economic importance for the lower Sylhet Basin (CEGIS 2012, Jakariya and Islam 2017). Although SWAT takes spatial variability within a sub-basin into account during HRU configuration, the model does not preserve the actual spatial address of the different components, including wetlands in the case of SWATrw, that are used in HRU definition. For a sub-basin-scale wetland, once the total volume of water in a wetland is simulated then inundation extent is calculated from the pre-specified volume–area–depth relationship (Equations (1) and (2)). As a result, simulated inundation extent represents the total inundated area of a wetland within a sub-basin without any spatial signature.

Simulated mean monthly wetland inundation extents in terms of inundation fraction (InFr, the ratio of mean monthly inundated area to its area at maximum capacity) are shown in Fig. 11. Results are provided for the baseline and the ensemble mean from the 17 GCMs for the future (2031–2050) period. The coefficient of variation across the 17 GCMs is also shown. For the baseline almost all haors in the basin are completely or nearly completely inundated to their maximum capacity (InFr ranges from 0.8 to 1.0) through the monsoon and post-monsoon seasons (June–November). At the beginning of the dry season (December), when rapid draining of haors usually occurs permitting planting of the next Boro rice crop, many of the haors are still relatively full (InFr: 0.6–1.0). The resulting delay in planting enhances the risk that Boro rice is damaged by flash floods in April/May prior to harvesting.

Figure 11 shows that inter-GCM variations in simulated InFr are generally relatively small (mostly within the 5% coefficient of variation band) but are larger (up to 30%) during the period April–June. The ensemble mean projects small increases in the extent of inundation (increases in InFr of 0.005–0.055) between January and April for all haors except some towards the upstream end of the Sylhet sub-basin near the Meghalaya sub-basin. The haors in the lower part of the Sylhet sub-basin commonly experience increases in inundated area compared to the baseline. This is possibly the result of an extension in the length of the period when haors are hydraulically connected to the two major converging rivers (the Surma and Kushiyara) in this part of the basin. In May and June, the majority of haors experience a decline in the area of inundation compared to the baseline (maximum change in InFr: 0.14). This decline could be indicative of a reduction in the risk to Boro rice cultivation especially in the upper part of the Sylhet sub-basin that experiences some of the largest changes.

*Figure 11*

Modelled annual baseline ET (not shown here) varies from 455 mm for the Meghalaya Basin to 631 mm for the Sylhet Basin. For all calendar months, the projected ensemble mean ET across most of the basin exceeds the corresponding baseline contributing to an increase in annual ET of between 1.2 and 4.7%. For the Sylhet Basin, although overall mean annual ET increases, lower ET (1–8%) is simulated between April and June. This reduction may be associated with a decline in the extent of haor inundation in these months. Such causality between inundation extent and ET has been observed for China's Poyang Lake wetland (Zhao and Liu 2014). Although rising temperature is projected to lead to an increase in regional PET demand (approx. 10.9 mm decade$^{-1}$) over the 21st century (Rahman *et al.* 2018), the availability of surface and/or near surface water will exert a critical control on actual ET. We conjecture that declining rainfall (and hence river discharge) and so a reduction in wetland inundation suppress ET over the haor region in the pre-monsoon season despite the increases in projected temperature that creates higher PET demands.


### *4.5 Projected risk of flood induced damage to Boro rice*

A particular objective of this study is to assess the risks associated with damage to the Boro rice crop by flash floods. As discussed above, this is a common occurrence immediately before and during the rice-harvesting period (April or May). A risk map was constructed from CDF curves of the simulated wetland water surface areas during

planting (December or January) and harvesting (April or May) periods (Fig. 12). Since there are 119 sub-basin

level wetlands in the model, the simulated daily water surface areas were summed across all wetlands to obtain the

total wetland inundation extent for each day of the simulation period. The cdfs in Fig. 12 were then constructed

from these basin-level daily wetland water extents for the corresponding months. A value of cdf corresponding to

a particular wetland area (or wetland depth, see Equation (1)) represents the inundation/submergence probability

of all areas at or below that wetland area (depth). Thus, the exceedance probability of that wetland area being at

risk of flooding is equal to 1 minus the corresponding cdf value (i.e. non-exceedance probability). A risk zone

(shaded in Fig. 12) demarcates the exceedence probabilities of wetland areas being at risk of flooding during the

harvesting period. Farmers transplant Boro rice seedlings to un-inundated haor areas during planting time (i.e.

December or January) (CEGIS 2012, Jakariya and Islam 2017). Therefore, the highest water level in a harvesting

month and the lowest water level in a planting month during a given period (e.g. 1981–2000 for the baseline) are

the two boundary points which define the largest possible wetland area that can be exposed to flash floods during

harvesting (also see Fig. S6). In Fig. 12(a), for example, the lowest inundated area during the planting month

(December) is $385 \times 10^3$ ha and the highest inundated area during the harvesting month (April) is $518 \times 10^3$ ha.

For the harvesting month, therefore, the potential flash flood exposed (PFFE) area will be equal to the difference

of the two extreme values (i.e. $133 \times 10^3$ ha). Since the area of a risk zone cannot be equal to the corresponding

PFFE area unless the exceedence probability is equal to 1.0, the flooding risk zone of a wetland can be normalized

with respect to its PFFE area. This is termed the rationalized flood risk (RFR). Therefore, the value of RFR

indicates the average flooding risk of a wetland. This can be used to compare flooding risks of different wetlands

and the flood risk associated with different scenarios.

*Figure 12*

Assuming that the traditional practice of transplanting Boro rice seedlings in December and then harvesting

rice in April will continue in the future, projected future flooding risk can be compared with that of the baseline

(Fig. 12(a) and (b)). Figure 12(b) is generated from the time series of daily ensemble mean haor inundated areas.

The average flooding risk (RFR value) of Boro rice for the baseline period is 0.12 (Fig. 12(a)). This decreases to 0

for the future (2031–2050) period (Fig. 12(b)), since no wetland areas are delineated as PFFE. According to its

definition, a wetland will not have any PFFE area unless the highest water level in a harvesting month exceeds the

lowest water level in the corresponding planting month. In Fig. 12(b), both these extreme values coincide at $444 \times$

$10^3$ ha. Although the projected average flooding risk decreases in the future, the permanent inundated area in December increases from the baseline value of $385 \times 10^3$ ha to $444 \times 10^3$ ha (15.3%). On one hand this reduces the extent of land that has potential for Boro rice cultivation, while on the other, increased water storage during the dry season could have beneficial ecological consequences such as providing habitat for fish with potential benefits for fisheries production (Miah *et al.* 2017). Enhanced dry season storage could also satisfy demands for irrigation water at this time of year (Hasan and Hossain 2013).

The above analysis was repeated assuming that planting (January) and harvesting (May) of Boro rice is delayed by one month (Fig. 12(c) and (d)). Although this farming practice is not generally followed in the haor region, it can occur under some circumstances: (i) limited drainage of a haor means that there is a relatively small area suitable for planting in December, and (ii) when temperatures are lower than normal it results in rice plants taking longer to mature (Mahmood 1997). This delayed planting / harvesting is associated with higher flood risk for both the baseline and future periods, as reflected in their RFR values of 0.41 and 0.39, respectively (i.e. a reduction in RFR of 0.02). Elevated risk is primarily associated with increases in the extent of the lower haor areas that are planted with rice. These lower areas have higher exceedence probability for flooding, thus increasing risk of damage. Moreover, delayed harvesting means that a larger area is inundated at this time further increasing the RFR values.

Regardless of farming practice, the Sylhet Basin is projected to lose cultivable area within its haors due to an increase in permanent wetland inundation in either of the two planting months (December or January). Given the significance of the rice crop to the economy of Bangladesh and the position of rice as the staple food of around 156 million Bangladeshis (Sarker *et al.* 2012, Shelley *et al.* 2016), such loss of cultivatable land could have important socio-economic consequences.

In order to protect Boro rice crops from flooding, the Government of Bangladesh is funding the construction of earth dykes around the periphery of many haors (CEGIS 2012). These dykes are generally low (1–3 m) and are designed to temporarily prevent rising river levels from flooding cultivated land at the very start of the monsoon. Subsequent overtopping enables the haors to flood, sustaining the associated natural processes such as deposition of fertile sediment, a critical resource in an area where marginal farmers cannot afford alternative artificial fertilizers. Such practices have been employed in other depressional wetlands within Asia including the Vietnamese Mekong Delta (Chapman and Darby 2016). However, dyke construction and the required maintenance

due to their frequent breaching are costly. Whilst the above analysis is based on the combined wetland inundation extent across the basin, it is possible to generate a risk map for individual haors, or a number of haors within geographically distinct areas. Given the existing financial constraints associated with dyke construction and maintenance, the approach developed in this study could be employed to identify and prioritize (e.g. through the RFR value) those haors that would be most suitable for such management interventions. In this way, the approach developed in this study could contribute to the on-going Master Plan of Haor Areas (CEGIS 2012) in Bangladesh.

## 5 Conclusions

This research was conceived to project the impacts of climate change on the UMRB and, in particular, to assesses the implications for flooding of Boro rice crops grown within the haor wetlands of the lower part of the basin. Results from the SWATrw model show that outflows from the basin during the wet season (April–November) are primarily governed by the flows from the Meghalaya catchment, the wettest of the upstream catchments. As such, underestimation of flows at Bhairab Bazar was likely caused by the under-representation of rainfall in the Meghalaya catchment. Both sets of rainfall data used for the Indian part of the basin (IMDgrid and IMDdist) were secondary data, rather than meteorological station records that were only available for Bangladesh. Whilst successive attempts to acquire such data were made, they were not successful. Cooperation between transboundary countries in exchanging data is essential to harness the maximum benefits from a shared catchment. In this case, the use of more reliable data for the upstream part of the UMRB has the potential to enhance model performance and would be a valuable future extension of this work.

This study has identified a potential limitation of SWATrw (also SWAT). The assumption of zero boundary flow conditions between aquifers of adjacent sub-basins can produce unrealistic results. This was most evident for the Laurergahr gauging station and may also be an issue in the low-lying Sylhet sub-basin that is underlain by continuous shallow aquifers. Incorporation of approaches to enable sub-basin level aquifer connectivity within SWAT/SWATrw would be required to address this issue.

This study has improved the QM bias-correction method by incorporating adjustments to dry day frequency (coldest day for temperature) in raw GCM rainfall (temperature) data for local-scale climate change studies. Whilst they are widely used, the delta factor, and the less frequently employed QM based approaches,

rarely address issues associated with the extreme lowest quantities (i.e. dry and coldest days) in raw GCM data. Adjustment of the lowest extremes is essential, especially when dry season hydrological responses to climate change are to be projected. The new QM approach has potential for wider applications in climate change studies.

Projected (2031–2050) ensemble mean (17 GCMs) inundation of haors in the lower part of the Sylhet sub-basin increases by up to 5.5% compared to the 1981–2000 baseline. Inundation of upstream haors is either unchanged or declines (by a maximum of 14% in May and June). The flood risk indicator developed in this study enables quantification of flooding risk for cultivated parts of the haor wetlands. Both of the Boro rice farming practices (December–April and January–May planting / harvesting) are projected to be less vulnerable to flash floods. Declines in the area exposed to flash floods are due to an increase in the lowest water levels at the time of rice planting and a reduction in the highest water levels when rice is harvested. As for the baseline period, under-projected climate change the January–May farming practice remains riskier than the December–April practice. Despite reductions in flash flood risk, increases in the area of permanent inundation produce a net loss in cultivable land of between $50 \times 10^3$ and $59 \times 10^3$ ha. These declines could have significant socio-economic implications.

# References

Acreman, M. C., Blake, J. R., Booker, D. J., Harding, R. J., Reynard, N., Mountford, J. O., and Stratford, C. J., 2009. A simple framework for evaluating regional wetland ecohydrological response to climate change with case studies from Great Britain. *Ecohydrology* **2**, 1–17. doi:10.1002/eco

Alam, Z. R., 2011. *Assessment of climate change impact on the Meghna River Basin using GBHM (Geomorphology Based Hydrological Model ).* Thesis (MS). Bangladesh University of Engineering and Technology.

Arnell, N. W., 2003. Effects of IPCC SRES emissions scenarios on river runoff: a global perspective. *Hydrology and Earth System Sciences* **7**(5), 619–641. doi:10.5194/hess-7-619-2003

ASCE, 1993. Criteria for evaluation of watershed models. *Journal of Irrigation and Drainange Engineering* 119(3), 429–442.

Ashfaq, M., Bowling, L. C., Cherkauer, K., Pal, J. S., and Diffenbaugh, N. S., 2010. Influence of climate model biases and daily-scale temperature and precipitation events on hydrological impacts assessment: A case study of the United States. *Journal of Geophysical Research* 115(14), 1–15. doi:10.1029/2009JD012965

Baki, A. B. M., Bari, M. F., and Haque, M. I., 2008. An analysis of upstream withdrawal scenarios using geo-spatial approach in the Surma-Kushiyara river basin. *Journal of Civil Engineering* 36(2), 97–109.

Baldassarre, G. Di and Montanari, A, 2009. Uncertainty in river discharge observations: a quantitative analysis. *Hydrology and Earth System Sciences Discuss.* 6(1), 39–61. doi:10.5194/hessd-6-39-2009

Basher, M. A., Stiller-reeve, M. A., Islam, A. K. M. S., and Bremer, S., 2018. Assessing climatic trends of extreme rainfall indices over northeast Bangladesh. *Theoretical and Applied Climatology* 134, 441–452.

Brooks, J. R., et al., 2018. Estimating wetland connectivity to streams in the Prairie Pothole region: An isotopic and remote sensing approach. *Water Resources Research* 54, 955–977.

Brown, M. E., et al., 2015. Climate change, global food security, and the U.S. food system. Retrieved from: https://www.usda.gov/oce/climate_change/FoodSecurity2015Assessment/FullAssessment.pdf [Accessed 6 November 2018]

Carolina, G. A. and Jackson, C. R., 2011. Potential impacts of climate change on groundwater supplies to the doñana wetland, Spain. *Wetlands* 31(5), 907–920. doi:10.1007/s13157-011-0205-4

CEGIS (Center for Environmental and Geographic Information Services), 2012. Master Plan of Haor Areas (Volume II), Vol. II. Dhaka: Center for Environmental and Geographic Information Services.

Chadwick, R., Good, P., Martin, G., and Rowell, D. P., 2015. Large rainfall changes consistently projected over substantial areas of tropical land. *Nature Climate Change* 6 (September), 177–182. doi:10.1038/nclimate2805

Chang, H. and Jung, I. W., 2010. Spatial and temporal changes in runoff caused by climate change in a complex large river basin in Oregon. *Journal of Hydrology* 388(3–4), 186–207. doi:10.1016/j.jhydrol.2010.04.040

Chapman, A. and Darby, S., 2016. Evaluating sustainable adaptation strategies for vulnerable mega-deltas using system dynamics modelling: Rice agriculture in the Mekong Delta's An Giang Province, Vietnam. *Science of The Total Environment* 559, 326–338. doi:10.1016/j.scitotenv.2016.02.162

Chowdhury, J. U. and Salehin, M., 1997. Floods and their processes. *Proceedings of an International Semininar on Evolution of Scientific System of Flood Forecasting and Warning in the Ganges, Brahmaputra and Meghna River Basins*, 247–254. Dhaka, Bangladesh: Bangladesh National Committee of International Commission for Irrigation and Drainage (ICID).

Chowdhury, M. R. and Ward, N., 2004. Hydro-meteorological variability in the greater Ganges-Brahmaputra-Meghna basins. *International Journal of Climatology* 24(12), 1495–1508. doi:10.1002/joc.1076

Coron, L., Andréassian, V., Perrin, C., Lerat, J., Vaze, J., Bourqui, M., and Hendrickx, F., 2012. Crash testing hydrological models in contrasted climate conditions: An experiment on 216 Australian catchments. *Water Resources Research* 48(5), 1-17. doi:10.1029/2011WR011721

Dai, A., Qian, T., Trenberth, K. E. and Milliman, J. D., 2009. Changes in continental freshwater discharge from 1948 to 2004. *Journal of Climate* 22(10), 2773–2792. doi:10.1175/2008JCLI2592.1

Dash, S. K., Sharma, N., Pattnayak, K. C., Gao, X. J., and Shi, Y., 2012. Temperature and precipitation changes in the north-east India and their future projections. *Global and Planetary Change* 98–99, 31–44. doi:10.1016/j.gloplacha.2012.07.006

Fadil, A., Rhinane, H., Kaoukaya, A., Kharchaf, Y., and Bachir, O. A., 2011. Hydrologic Modeling of the Bouregreg Watershed (Morocco) Using GIS and SWAT Model. *Journal of Geographic Information System* 03(04), 279–289. doi:10.4236/jgis.2011.34024

Feng, X. Q., Zhang, G. X., and Jun Xu, Y., 2013. Simulation of hydrological processes in the Zhalong wetland

within a river basin, Northeast China. *Hydrology and Earth System Sciences* 17(7), 2797–2807. doi:10.5194/hess-17-2797-2013

Fox, J., Mustafa, M. G., Quazi, S. A., Miles, W. B., Cunningham, E. J., and Chassels, M., 2011. *Rural livelihoods and protected landscapes: co-management in the wetlands and forests of Bangladesh*. Dhaka: Nishorgo Network.

Gopal, B., 2013. Future of wetlands in tropical and subtropical Asia, especially in the face of climate change. *Aquatic Science* 75, 39–61. doi:10.1007/s00027-011-0247-y

Greenberg, C. H., Goodrick, S., Austin, J. D., and Parresol, B. R., 2015. Hydroregime prediction models for ephemeral groundwater-driven sinkhole wetlands: a planning tool for climate change and amphibian conservation. *Wetlands* 35(5), 899–911. doi:10.1007/s13157-015-0680-0

Hanasaki, N., et al., 2008. An integrated model for the assessment of global water resources – Part 2: Applications and assessments. *Hydrology and Earth System Sciences* 12(4), 1027–1037. doi:10.5194/hess-12-1027-2008

Hansen, M. C., Defries, R. S., Townshend, J. R. G., and Sohlberg, R., 2000. Global land cover classification at 1 km spatial resolution using a classification tree approach. *International Journal of Remote Sensing* 21(6), 1331–1364.

Harris, I., Jones, P. D., Osborn, T. J., and Lister, D. H., 2014. Updated high-resolution grids of monthly climatic observations - the CRU TS3.10 Dataset. *International Journal of Climatology* 34(3), 623–642. doi:10.1002/joc.3711

Hasan, M. R. and Hossain, A. F. M. A., 2013. Surface water potentiality for minor irrigation expansion in haor areas of Bangladesh. *International Journal of Civil Engineering* 2(3), 13–20.

Hayashi, M. and Kamp, G. van der., 2000. Simple equations to represent the volume–area–depth relations of shallow wetlands in small topographic depressions. *Journal of Hydrology* 237(1–2), 74–85. doi:10.1016/S0022-1694(00)00300-0

Hidayat, H., Vermeulen, B., Sassi, M. G., Torfs, P. J. J. F., and Hoitink, A. J. F., 2011. Discharge estimation in a backwater affected meandering river. *Hydrology and Earth System Sciences* 15(8), 2717–2728. doi:10.5194/hess-15-2717-2011

Hurkmans, R. T. W. L., Terink, W., Uijlenhoet, R., Moors, E. J., Troch, P. A. & Verburg, P. H., 2009. Effects of land use changes on streamflow generation in the Rhine basin. *Water Resources Research* 45(6), 1–15. doi:10.1029/2008WR007574

Hudson, C.E. and Thompson, J.R., 2019. Hydrological modelling of climate change impacts on river flows in Siberia's Lena River Basin and implications for the Atlantic Meridional Overturning Circulation. *Hydrology Research* doi: 10.2166/nh.2019.151

Hwang, S. and Graham, W. D., 2013. Development and comparative evaluation of a stochastic analog method to downscale daily GCM precipitation. *Hydrology and Earth System Sciences* 17(11), 4481–4502. doi:10.5194/hess-17-4481-2013

Hwang, S. and Graham, W. D., 2014. Assessment of alternative methods for statistically downscaling daily GCM precipitation outputs to simulate regional streamflow. *Journal of the American Water Resources Association* 50(4), 1010–1032. doi:10.1111/jawr.12154

Immerzeel, W., 2008. Historical trends and future predictions of climate variability in the Brahmaputra basin. *International Journal of Climatology* 28(2), 243–254. doi:10.1002/joc

Ines, A. V. M. and Hansen, J. W., 2006. Bias correction of daily GCM rainfall for crop simulation studies. *Agricultural and Forest Meteorology* 138(1–4), 44–53. doi:10.1016/j.agrformet.2006.03.009

IPCC, 2013. *Climate Change 2013: The Physical Science Basis.* Contribution of Working Group I to the Fifth Assessment Report of the Intergovernmental Panel on Climate Change. T. F. Stocker, *et al*., Eds.). Cambridge, UK and New York, NY: Cambridge University Press.

Islam, S. N., 2010. Threatened wetlands and ecologically sensitive ecosystems management in Bangladesh. *Frontiers in Earth Sciences China* 4(4), 438–448. doi:10.1007/s11707-010-0127-0

Jakariya, M. and Islam, M. N., 2017. Evaluation of climate change induced vulnerability and adaptation strategies at Haor areas in Bangladesh by integrating GIS and DIVA model. *Modelling Earth Systems and Environment* 3(4), 1303–1321. doi:10.1007/s40808-017-0378-9

Jha, L. K., 2017. Goal of becoming a developed nation by 2041. *Dhaka Tribune,* 26 April. Retrieved from: http://www.dhakatribune.com/bangladesh/2017/04/26/goal-becoming-developed-nation-2041/ [Accessed 17 June 2018]

Johnson, W. C., et al., 2010. Prairie wetland complexes as landscape functional units in a changing climate. *Bioscience* 60(2), 128–140. doi:10.1525/bio.2010.60.2.7

Junk, W. J., et al., 2013. Current state of knowledge regarding the world's wetlands and their future under global climate change: a synthesis. *Aquatic Science* 75(1), 151–167. doi:10.1007/s00027-012-0278-z

Karim, F., et al., 2015. Assessing the impacts of climate change and dams on floodplain inundation and wetland connectivity in the wet-dry tropics of northern Australia. *Journal of Hydrology* 522, 80–94. doi:10.1016/j.jhydrol.2014.12.005

Karim, F., *et al.*, 2016. Impact of climate change on floodplain inundation and hydrological connectivity between wetlands and rivers in a tropical river catchment. *Hydrology and Earth System Sciences* 30, 1574–1593. doi:10.1002/hyp.10714

Khan, A. S., Masud, A. S., and Palash, W., 2005. Hydrological impact study of Tipaimukh Dam Project of India on Bangladesh. Dhaka: Institute of Water Modelling.

Khan, M. N. H., Mia, M. Y., and Hossain, M. R., 2012. Impacts of flood on crop production in haor areas of two upazillas in Kishoregonj. *Journal of Environmental Science and Natural Resources* 5(1), 193–198.

Khoi, D. N. and Suetsugi, T., 2014. Impact of climate and land-use changes on hydrological processes and sediment yield—a case study of the Be River catchment, Vietnam. *Hydrological Sciences Journal* 59(5), 1095–1108. doi:10.1080/02626667.2013.819433

Leander, R. and Buishand, T. A., 2007. Resampling of regional climate model output for the simulation of extreme river flows. *Journal of Hydrology* 332(3–4), 487–496. doi:10.1016/j.jhydrol.2006.08.006

Lee, S., Wallace, C. W., Sadeghi, A. M., McCarty, G. W., Zhong, H., and Yeo, I. Y., 2018. Impacts of Global Circulation Model (GCM) bias and WXGEN on modeling hydrologic variables. *Water* 10(6). doi:10.3390/w10060764

Lehner, B., 2005. HydroSHEDS technical documentation, Version 1.0. World Wildlife Fund US, Washington, DC. Retrieved from: http://hydrosheds.cr.usgs.gov [Accessed 30 September 2019]

Li, H., Beldring, S., and Xu, C., 2015. Stability of model performance and parameter values on two catchments facing changes in climatic conditions. *Hydrological Sciences Journal 60 (7–8):1317–1330.* doi:10.1080/02626667.2014.978333

Li, Q., et al., 2016. Building Asian climate change scenario by multi-regional climate models ensemble. Part II: mean precipitation. *International Journal of Climatology* 36(13), 4241–4252. doi:10.1002/joc.4633

Liu, J., Williams, J. R., Wang, X., and Yang, H., 2009. Using MODAWEC to generate daily weather data for the EPIC model. *Environmental Modeling and Software* 24(5), 655–664. doi:10.1016/j.envsoft.2008.10.008

Liu, Y., Yang, W., and Wang, X., 2008. Development of a SWAT extension module to simulate riparian wetland hydrologic processes at a watershed scale. *Hydrological Processes* 22, 2901–2915. doi:10.1002/hyp

Lutz, A. F., Maat, H. W. ter, Biemans, H., Shrestha, A. B., Wester, P., and Immerzeel, W. W., 2016. Selecting representative climate models for climate change impact studies: An advanced envelope-based selection approach. *International Journal of Climatology* doi:10.1002/joc.4608

Mahmood, R., 1997. Impacts of air temperature variations on the boro rice phenology in Bangladesh: implications for irrigation requirements. *Agricultural and Forest Meteorology* 84, 233–247.

Masood, M. and Takeuchi, K., 2016. Climate change impacts and its implications on future water resource management in the Meghna Basin. *Futures* 78–79, 1–18. doi:10.1016/j.futures.2016.03.001

Masood, M., Yeh, P. J.-F., Hanasaki, N., and Takeuchi, K., 2015. Model study of the impacts of future climate change on the hydrology of Ganges-Brahmaputra-Meghna basin. *Hydrology and Earth System Sciences* 19(2), 747–770. doi:10.5194/hess-19-747-2015

McCartney, M., Rebelo, L.-M., Senaratna Sellamuttu, S., and Silva, S. de., 2010. Wetlands, agriculture and poverty reduction. Colombo, Sri Lanka: International Water Management Institute. doi:10.5337/2010.230

Meinshausen, M., et al., 2011. The RCP greenhouse gas concentrations and their extensions from 1765 to 2300. *Climatic Change* 109, 213–241. doi:10.1007/s10584-011-0156-z

Merz, R., Parajka, J., and Blöschl, G., 2011. Time stability of catchment model parameters: Implications for climate impact analyses. *Water Resources Research* 47(2), 1-17. doi:10.1029/2010WR009505

Miah, M. I., Zahan, N., Mondal, D. K., Uddin, M. J., and Halim, M. A., 2017. Management of beel fishery: a special reference to Chapaigachi beel of Kushtia, Bangladesh. *Journal of Bioscience and Agricultural Research* 13(2), 1122–1129.

Moffitt, C. B., Hossain, F., Adler, R. F., Yilmaz, K. K., and Pierce, H. F., 2011. Validation of a TRMM-based global Flood Detection System in Bangladesh. *International Journal of Applied Earth Obsveration and Geoinformation* 13(2), 165–177. doi:10.1016/j.jag.2010.11.003

Mohamed, Y. and Savenije, H. H. G., 2014. Impact of climate variability on the hydrology of the Sudd wetland: signals derived from long term (1900-2000) water balance computations. *Wetlands Ecology and Management*

22(2), 191–198. doi:10.1007/s11273-014-9337-7

Molla, M. H. R., Islam, M. S., Rahman, M. A., Lee, S. G., Jahan, B., Iqbal, J., and Mamtaz, S., 2018. An assessment of geo-morphology and hydro-biological factors of major wetlands of Bangladesh. *Water Science and Technology* 78(3), 578–587. doi:10.2166/wst.2018.328

Moriasi, D. N., Arnold, J. G., Liew, M. W. Van, Bingner, R. L., Harmel, R. D., and Veith, T. L., 2007. Model evaluation guidelines for systematic quatification of accuracy in watershed simulations. *Transactions of the American Society of Agricultural and Biological Engineers* 50(3), 885–900.

Murray, S. J., Foster, P. N. and Prentice, I. C., 2012. Future global water resources with respect to climate change and water withdrawals as estimated by a dynamic global vegetation model. *Journal of Hydrology* 448–449, 14–29. doi:10.1016/j.jhydrol.2012.02.044

Nash, J. E. and Sutcliffe, J. V., 1970. River flow forecasting through conceptual models. Part I: a discussion of principles. *Journal of Hydrology* 10(3), 282–290.

Nath, A. J. and Lal, R., 2017. Managing tropical wetlands for advancing global rice production : Implications for land-use management. *Land Use Policy*. 68, 681–685.

Neitsch, S. L., Arnold, J. G., Kiniry, J. R., and Williams, J. R., 2011. Soil and Water Assessment Tool, Theoretical Documentation, Version 2009. College Station, TX: US Department of Agriculture - Agricultural Research Service, Grassland, Soil and Water Research Laboratory.

Neupane, R. P. and Kumar, S., 2015. Estimating the effects of potential climate and land use changes on hydrologic processes of a large agriculture dominated watershed. *Journal of Hydrology* 529, 418–429.

Nishat, B. and Rahman, S. M. M., 2009. Water resources modeling of the Ganges-Brahmaputra-Meghna River Basins using satellite remote sensing data. *Journal of the American Water Resources Association* 45(6), 1313–1327. doi:10.1111/j.1752-1688.2009.00374.x

Nungesser, M., Saunders, C., Coronado-Molina, C., Obeysekera, J., Johnson, J., McVoy, C., and Benscoter, B., 2015. Potential effects of climate change on Florida's Everglades. *Environmental Management* 55(4), 824–835. doi:10.1007/s00267-014-0417-5

Ouyang, F., Zhu, Y., Fu, G., and Chen, X., 2015. Impacts of climate change under CMIP5 RCP scenarios on streamflow in the Huangnizhuang catchment. *Stochastic Environmental Research and Risk Assessment* 29(7), 1781–1795. doi:10.1007/s00477-014-1018-9

Palmer, M. A., Liermann, C. A. R., Nilsson, C., Flörke, M., Alcamo, J., Lake, P. S. & Bond, N., 2008. Climate change and the world's river basins: anticipating management options. *Frontiers in Ecology and the Environment* 6(2), 81–89. doi:10.1890/060148

Pan, S., et al., 2015. Responses of global terrestrial evapotranspiration to climate change and increasing atmospheric CO2 in the 21st century. *Earth' s Future* 3, 15–35. doi:10.1002/2014EF000263

Pitchford, J. L., et al., 2012. Climate change effects on hydrology and ecology of wetlands in the mid-atlantic highlands. *Wetlands* 32(1), 21–33. doi:10.1007/s13157-011-0259-3

Poggio, L. and Soille, P., 2011. A probabilistic approach to river network detection in digital elevation models. *Catena* 87(3), 341–350. doi:10.1016/j.catena.2011.07.001

Ponce, V. M. (1989) *Engineering hydrology: principles and practices*. NJ: Prentice Hall.

Popescu, I., Cioaca, E., Pan, Q., Jonoski, A., and Hanganu, J., 2015. Use of hydrodynamic models for the management of the Danube Delta wetlands : The case study of Sontea-Fortuna ecosystem. *Environmental Science and Policy* 46, 48–56.

Quan, N. H., et al., 2018. Conservation of the Mekong Delta wetlands through hydrological management. *Ecological Research* 33(1), 87–103. doi:10.1007/s11284-017-1545-1

Rahman, M. A., Yunsheng, L., Sultana, N., and Ongoma, V., 2018. Analysis of reference evapotranspiration - (ET0) trends under climate change in Bangladesh using observed and CMIP5 data sets. *Meteorological and Atmospheric Physics* 1–17. doi:10.1007/s00703-018-0596-3

Rahman, M. M., Singh Arya, D., Goel, N. K., and Mitra, A. K., 2012. Rainfall statistics evaluation of ECMWF model and TRMM data over Bangladesh for flood related studies. *Meteorological Applications* 19(4), 501–512. doi:10.1002/met.293

Rahman, M. M., Thompson, J. R., and Flower, R. J., 2016. An enhanced SWAT wetland module to quantify hydraulic interactions between riparian depressional wetlands, rivers and aquifers. *Environmental Modelling and Software* 84, 263–289. doi:10.1016/j.envsoft.2016.07.003

Ramsar Convention on Wetlands, 2018. Global Wetland Outlook: State of the World's Wetlands and their Services to People. Gland, Switzerland: Ramsar.

Rashid, M. M., Beecham, S., and Chowdhury, R. K., 2015. Statistical downscaling of CMIP5 outputs for

projecting future changes in rainfall in the Onkaparinga catchment. *Science of The Total Environment* 530–531(2015), 171–182. doi:10.1016/j.scitotenv.2015.05.024

RRCAP, 2001. State of the Envirionment Report: Bangladesh 2001. Klong Luang. Retrieved from: http://www.rrcap.ait.asia/Publications/bangladesh%20soe.pdf [Accessed 2 February 2019]

Sarker, M. A. R., Alam, K., and Gow, J., 2012. Exploring the relationship between climate change and rice yield in Bangladesh: An analysis of time series data. *Agricultural Systems* 112, 11–16.

Sarker, M. A. R., Alam, K., and Gow, J., 2017. Performance of rain-fed Aman rice yield in Bangladesh in the presence of climate change. *Renewable Agriculture and Food Systems* 1–9. doi:10.1017/s1742170517000473

Schneider, C., Laizé, C. L. R., Acreman, M. C. and Flörke, M., 2013. How will climate change modify river flow regimes in Europe? *Hydrology and Earth System Sciences* 17(1), 325–339. doi:10.5194/hess-17-325-2013

Seibert, J., 2003. Reliability of model predictions outside calibration conditions. *Nordic Hydrology* 34, 477–492.

Sharpley, A. N. and Williams, J. R., 1990. EPIC-Erosion Productivity Impact Calculator, 1. Model Documentation. US Department of Agriculture, Agricultural Research Service.

Shelley, I. J., Takahashi-Nosaka, M., Kano-Nakata, M., Haque, M. S., and Inukai, Y., 2016. Rice cultivation in Bangladesh : Present scenario , problems , and prospects. *Journal of International Cooperation for Agricultural Development* 14, 20–29.

Sherwood, D. B., 2009. Community-based wetland comanagement in Bangladesh. In: K.M. Moore, ed., *The sciences and art of adaptive management: innovating for sustainable agriculture and natural resource management* Ankeny, IA: Soil and Water Conservation Society. Retrieved from: http://www.swcs.org/documents/filelibrary/adaptive_management/AdaptiveChapter9_926CF14F470BC.pdf

Shrestha, R. R., Dibike, Y. B., and Prowse, T. D., 2012. Modeling Climate Change Impacts on Hydrology and Nutrient Loading in the Upper Assiniboine Catchment. *Journal of the American Water Resources Association* 48(1), 74–89. doi:10.1111/j.1752-1688.2011.00592.x

Singh, C. R., Thompson, J. R., French, J. R., Kingston, D. G., and Mackay, A. W., 2010. Modelling the impact of prescribed global warming on runoff from headwater catchments of the Irrawaddy River and their implications for the water level regime of Loktak Lake, northeast India. *Hydrology and Earth System Sciences* 14(9), 1745–1765. doi:10.5194/hess-14-1745-2010

Strzepek, K., McCluskey, A., Boehlert, B., Jacobsen, M. and Fant IV, C., 2011. Climate variability and change: A basin scale indicator approach to understanding the risk to water resources development and management. Washington DC: World Bank.

Sulis, M., Paniconi, C., Marrocu, M., Huard, D., and Chaumont, D., 2012. Hydrologic response to multimodel climate output using a physically based model of groundwater/surface water interactions. *Water Resources Research* 48(12), 1–18. doi:10.1029/2012WR012304

Sun, C., Zhen, L., and Miah, M. G., 2017. Comparison of the ecosystem services provided by China's Poyang Lake wetland and Bangladesh's Tanguar Haor wetland. *Ecosystem Services* 26, 411–421.

Tang, J., et al., 2016. Building Asian climate change scenario by multi-regional climate models ensemble. Part I: surface air temperature. *International Journal of Climatology* 36(13), 4241–4252. doi:10.1002/joc.4628

Tang, Q. and Lettenmaier, D. P., 2012. 21st century runoff sensitivies of major global river basins. *Geophysical Research Letters* 39(6), 1–5. doi:10.1029/2011GL050834

Themeßl, M. J., Gobiet, A., and Heinrich, G., 2012. Empirical-statistical downscaling and error correction of regional climate models and its impact on the climate change signal. *Climatic Change* 112(2), 449–468. doi:10.1007/s10584-011-0224-4

Thompson, J. R., Crawley, A., and Kingston, D. G., 2016. GCM-related uncertainty for river flows and inundation under climate change: the Inner Niger Delta. *Hydrological Sciences Journal* 61(13), 2325–2347. doi:10.1080/02626667.2015.1117173

Thompson, J. R., Crawley, A., and Kingston, D. G., 2017a. Future river flows and flood extent in the Upper Niger and Inner Niger Delta: GCM-related uncertainty using the CMIP5 ensemble. *Hydrological Sciences Journal* 62(14), 2239–2265. doi:10.1080/02626667.2017.1383608

Thompson, J. R., Green, A. J., and Kingston, D. G., 2014. Potential evapotranspiration-related uncertainty in climate change impacts on river flow: An assessment for the Mekong River basin. *Journal of Hydrology* 510, 259–279. doi:10.1016/j.jhydrol.2013.12.010

Thompson, J. R., *et al.*,2017b. Simulation of the hydrological impacts of climate change on a restored floodplain. *Hydrological Sciences Journal* 62(15), 2482–2510. doi:10.1080/02626667.2017.1390316

Thompson, P. and Balasinorwala, T., 2010. Wetland management and conservation , Hail Haor, Bangladesh. Retrieved from: http://www.teebweb.org/wp-content/uploads/CaseStudies/Wetland management and

conservation, Hail Haor, Bangladesh.pdf [Accessed 20 June 2017]

UNFCCC (United Nations Framework Convention on Climate Change), 2015. Adoption of the Paris Agreement, 21st Conference of the Parties. Paris, France. Retrieved from: https://unfccc.int/process/the-paris-agreement/status-of-ratification [Accessed 26 September 2019]

Velázquez, J. A., et al., 2013. An ensemble approach to assess hydrological models' contribution to uncertainties in the analysis of climate change impact on water resources. *Hydrology and Earth System Sciences* 17, 565–578. doi:10.5194/hess-17-565-2013

Wang, X., Yang, W., and Melesse, A. M., 2008. Using hydrologic equivalent wetland concept within SWAT to estimate streamflow in watersheds with numerous wetlands. *Transactions of the American Society of Agricultural and Biological Engineers* 51(1), 55–72. doi:10.13031/2013.24227

Wu, C. L., Shukla, S., and Shrestha, N. K., 2016. Evapotranspiration from drained wetlands with different hydrologic regimes: Drivers, modeling, and storage functions. *Journal of Hydrology* **538**, 416–428. doi:10.1016/j.jhydrol.2016.04.027

Yan, B., Fang, N. F., Zhang, P. C., and Shi, Z. H., 2013. Impacts of land use change on watershed streamflow and sediment yield: An assessment using hydrologic modelling and partial least squares regression. *Journal of Hydrology* 484, 26–37. doi:10.1016/j.jhydrol.2013.01.008

Yan, D., Werners, S.E., Ludwig, F., and Huang, H.Q., 2015. Hydrological response to climate change: The Pearl River, China under different RCP scenarios. *Journal of Hydrology Regional Studies* 4, 228–245.

Zhao, X. and Liu, Y., 2014. Lake fluctuation effectively regulates wetland evapotranspiration: A case study of the largest freshwater lake in China. *Water* 6, 2482–2500. doi:10.3390/w6082482

Zhu, Q., Zhang, X., Ma, C., Gao, C., and Xu, Y.-P., 2016. Investigating the uncertainty and transferability of parameters in SWAT model under climate change. *Hydrological Sciences Journal* 61(5), 914–930. doi:10.1080/02626667.2014.1000915

**Table 1.** Sources and characteristics of data used in the SWATrw model of the UMRB. DEM: digital elevation model; LULC: land use and land cover; HydroSHEDS: Hydrological data and maps based on Shuttle Elevation Derivatives at multiple Scales; CRU TS: Climatic Research Unit – University of East Anglia Time Series; FAO: Food and Agriculture Organization of the United Nations; SRTM: Shuttle Radar Topography Mission; AVHRR: Advanced Very High Resolution Radiometer;

| Data | Sources | Characteristics |
|---|---|---|
| DEM | HydroSHEDS database[2] (Lehner 2005) | Derived from the SRTM data, 90 m horizontal resolution |
| LULC | Global Land Cover (GLC) dataset[3] | Derived from AVHRR satellite imagery data (Hansen *et al.* 2000), 1 km horizontal resolution |
| Soil | Harmonized World Soil Database (HWSD)[4] | Provides major physico-chemical properties of soils (e.g. texture, gravel, bulk density, organic matter and pH) at 1 km horizontal resolution for two vertical layers: 0–300 and 300–1000 mm |
| Rainfall | Bangladesh Meteorological Department (BMD) and Bangladesh Water Development Board (BWDB) | Point daily rainfall measured at meteorological stations (see Fig. 1(a)) covering the periods 1981–2010 (BMD) and 1990–2010 (BWDB) for the Bangladeshi part of the basin |
| | Indian Meteorological Department (IMD) | Gridded (50 km × 50 km) daily rainfall (IMDgrid in Fig. 1(a)) for the period 1981–2005 and covering the Indian part of the basin |
| | IMD | District-wise average monthly rainfall (IMDdist in Fig. 1(a)) for the period 2004–2010 and covering the Indian part of the basin |
| | CRU TS 3.20 climate database (Harris *et al.* 2014) archived in the British Atmospheric Data Centre[5] | Gridded (50 km × 50 km) monthly rainfall for the period 1981–2010 and covering the whole basin |
| Temperature | BMD | Point daily data measured at BMD meteorological stations for the period 1981–2010 and covering the Bangladeshi part of the basin |
| | CRU TS 3.20 climate database | Gridded (50 km × 50 km) monthly mean temperature for the period 1987–2010 and covering the Indian part of the basin |
| Humidity, wind speed and solar radiation | CLIMWAT 2.0 database of FAO | Point data at available meteorological stations in the database comprising long time mean monthly values and covering the whole basin |
| River discharge | BWDB | BWDB generates daily discharge data from their rating curves using measured daily river stage. Data cover the period 1990–2010 |

---

[2] http://hydrosheds.cr.usgs.gov/index.php

[3] http://glcf.umd.edu/data/landcover/

[4] http://www.fao.org/soils-portal/soil-survey/soil-maps-and-databases/harmonized-world-soil-database-v12/en/

[5] http://badc.nerc.ac.uk/data/

**Table 2.** Calibration parameters and their final values in the SWATrw model of the UMRB. Parameters are grouped based on spatial scales (basin, sub-basin and HRU). Basin level parameter indicates that all HRUs in the basin use the same value of that parameter.

| Parameter | Description (unit) | Default value | Calibrated value |
|---|---|---|---|
| *Basin level* | | | |
| SURLAG | Surface runoff lag coefficient (day) | 4.00 | 0.10 |
| | | | |
| *HRU level* | | | |
| CN2 | Curve number | 70–92 | 47–95 |
| ESCO | Soil evaporation compensation factor | 0.95 | 0.0–0.95 |
| EPCO | Plant uptake compensation factor | 1.00 | 0.00–1.00 |
| GW_DELAY | Groundwater delay (day) | 31 | 1–61 |
| ALPHA_BF | Baseflow factor (day) | 0.048 | 0.01–0.70 |
| SHALLST | Initial depth of water in shallow aquifer (mm) | 0.50 | 0.00–1520.00 |
| GWQMN | Threshold depth of water in shallow aquifer for baseflow (mm) | 0.00 | 0.00–1480.00 |
| REVAPMN | Threshold depth of water in shallow aquifer for revap (mm) | 1.00 | 0.00–2000.00 |
| RCHRG_DP | Fraction of soil percolated water to deep aquifer | 0.05 | 0.00–0.80 |
| GW_SPYLD | Specific yield of shallow aquifer | 0.003 | 0.003–0.02 |
| | | | |
| *Sub-basin level* | | | |
| CH_N2 | Manning's roughness coefficient for a river | 0.014 | 0.001–0.06 |
| TRANS_AMT | Fraction of flow of a reach to be transferred to its immediate downstream distributary | | 0.1–0.9 |
| WET_FR | Fraction of sub-basin area drained into a wetland | - | 0.81–1.00 |
| WET_MXSA[b] | Maximum wetland water surface area (ha) | - | 5–29509 |
| WETEVCOEF | Wetland evaporation coefficient | - | 0.7 |
| WET_K | Hydraulic conductivity of wetland bottom (mm/h) | - | 0.30–8.00 |
| WET_D[a] | Initial wetland water depth (m) | - | 1.00 |
| WET_DMX[a,b] | Maximum wetland water depth (m) | - | 3.00–8.00 |
| WET_P[a] | Wetland shape factor | - | 0.9–1.5 |
| WET_TH[a,b] | Thickness of wetland bottom (m) | - | 1.00 |
| CCH_M[a,b] | Depth exponent in connecting channel flow equation | - | 2.00 |
| CCH_N[a,b] | Slope exponent in connecting channel flow equation | - | 1.00 |
| CCH_SF[a,b] | Friction slope of connecting channel | - | 0.01 |
| CCH_DFR[a] | Fraction of main channel maximum depth at normal level | - | 0.10–0.80 |
| CCH_LFR[a] | Fraction of main channel length to be overflowed at normal level | - | 0.10–0.90 |
| CCH_C[a] | Conveyance coefficient of connecting channel (m$^{-1}$ s$^{-1}$) | - | 667.00 |

[a]Newly incorporated parameters in SWATrw
[b]Not calibrated, rather parameter values were taken from available data, the literature and in some cases approximated based on the authors' detailed knowledge of the study area.

**Table 3.** Selected CMIP5 GCMs used in this study.

| CMIP5 GCM | Developer | Spatial resolution[a] (Lat × Long) |
|---|---|---|
| ACCESS1.0 | CSIRO (Commonwealth Scientific and Industrial Research Organization, Australia) and BOM (Bureau of Meteorology, Australia) | 1.25×1.88 |
| BCC-CSM1.1 | Beijing Climate Centre, China Meteorological Administration | 2.79×2.81 |
| BNU-ESM | College of Global Change and Earth System Science, Beijing Normal University, China | 2.79×2.81 |
| CanESM2 | Canadian Centre for Climate Modelling and Analysis | 2.79×2.81 |
| CCSM4 | National Center for Atmospheric Research, USA | 0.94×1.25 |
| CESM1-BGC | National Science Foundation, Department of Energy, National Center for Atmospheric Research | 0.94×1.25 |
| CNRM-CM5 | Centre National de Recherches Météorologiques | 1.40×1.41 |
| CSIRO-Mk3.6.0 | Commonwealth Scientific and Industrial Research Organization in collaboration with the Queensland Climate Change Centre of Excellence, Australia | 1.87×1.88 |
| GFDL-CM3 | Geophysical Fluid Dynamics Laboratory | 2.00×2.50 |
| GFDL-ESM2M | | 2.02×2.50 |
| IPSL-CM5A-LR | Institut Pierre-Simon Laplace | 1.89×3.75 |
| IPSL-CM5A-MR | | 1.27×2.50 |
| MIROC5 | Atmosphere and Ocean Research Institute (The University of Tokyo), National Institute for Environmental Studies, and Japan Agency for Marine-Earth Science and Technology | 1.40×1.41 |
| MIROC-ESM | Japan Agency for Marine-Earth Science and Technology, Atmosphere and Ocean Research Institute (The University of Tokyo), and National Institute for Environmental Studies | 2.79×2.81 |
| MIROC-ESM-CHEM | | 2.79×2.81 |
| MPI-ESM-LR | Max Planck Institute for Meteorology, Germany | 1.87×1.88 |
| MPI-ESM-MR | | 1.87×1.88 |
| NorESM1-M | Meteorological Research Institute Norwegian Climate Centre | 0.94×1.25 |

[a]The original spatial resolution of the GCM used to generate climate data.

**Table 4.** Model performance metrics for simulated monthly and daily (parenthesized) streamflow for the calibration (1990–2003) and validation (2004–2010) periods. NSE: Nash-Sutcliffe Efficiency; RSR: ratio of root mean square error to the standard deviation of observed data; $R^2$: coefficient of determination; PBIAS: percent bias.

| Gauging station (ID number) | Period | Performance statistics for monthly (daily) discharge | | | | Remarks[a] |
|---|---|---|---|---|---|---|
| | | NSE | RSR | $R^2$ | PBIAS | |
| Sheola (11) | Calibration | 0.76 (0.72) | 0.49 (0.53) | 0.82 (0.78) | –13.06 (–13.11) | G (G) |
| | Validation | 0.88 (0.73) | 0.34 (0.52) | 0.90 (0.76) | 5.33 (3.85) | VG (G) |
| Kanairghat (12) | Calibration | 0.88 (0.83) | 0.34 (0.42) | 0.88 (0.83) | 0.99 (0.3) | VG (VG) |
| | Validation | 0.88 (0.76) | 0.35 (0.49) | 0.89 (0.77) | 12.72 (10.86) | G (G) |
| Sarighat (3) | Calibration | 0.84 (0.75) | 0.40 (0.50) | 0.85 (0.78) | 6.60 (6.05) | VG (VG) |
| | Validation | 0.33 (–0.07) | 0.82 (0.20) | 0.61 (0.24) | 51.22 (64.20) | US (US) |
| Jaflong (4) | Calibration | 0.89 (0.70) | 0.32 (0.55) | 0.90 (0.77) | 2.68 (2.62) | VG (G) |
| | Validation | 0.90 (–0.39) | 0.31 (1.18) | 0.91 (0.20) | 7.51 (7.02) | VG (US) |
| Islampur (1) | Calibration | 0.75 (0.41) | 0.50 (0.77) | 0.77 (0.42) | 13.12 (14.63) | G (US) |
| | Validation | 0.61 (0.00) | 0.62 (1.00) | 0.84 (0.26) | 42.15 (41.87) | US (US) |
| Laurergahr (9) | Calibration | 0.61 (0.44) | 0.62 (0.75) | 0.70 (0.47) | –5.80 (–5.83) | S (US) |
| | Validation | 0.90 (0.59) | 0.32 (0.64) | 0.91 (0.60) | 9.03 (8.88) | VG (S) |
| Durgapur (7) | Calibration | 0.83 (0.47) | 0.41 (0.73) | 0.86 (0.49) | 12.38 (12.37) | G (US) |
| | Validation | =- | - | - | - | - |
| JariaJanjail (10) | Calibration | 0.77 (0.79) | 0.48 (0.46) | 0.82 (0.80) | –9.30 (7.21) | VG (VG) |
| | Validation | 0.54 (0.73) | 0.68 (0.52) | 0.71 (0.74) | –31.59 (–2.05) | US (S) |
| Jaldhup (8) | Calibration | 0.71 (0.73) | 0.54 (0.52) | 0.87 (0.85) | 20.88 (19.17) | S (S) |
| | Validation | 0.62 (0.59) | 0.62 (0.64) | 0.62 (0.59) | 7.30 (–0.55) | S (S) |
| Manu (6) | Calibration | 0.77 (0.56) | 0.48 (0.67) | 0.78 (0.56) | –5.27 (–2.48) | VG (S) |
| | Validation | 0.74 (0.17) | 0.51 (0.91) | 0.76 (0.26) | 5.68 (0.61) | G (US) |
| Kamalganj (2) | Calibration | 0.23 (0.24) | 0.88 (0.87) | 0.67 (0.40) | –48.74 (–44.87) | US (US) |
| | Validation | 0.25 (0.19) | 0.87 (0.90) | 0.61 (0.34) | –20.26 (–3.51) | US (US) |
| Sherpur (14) | Calibration | 0.69 (0.65) | 0.55 (0.59) | 0.87 (0.83) | –18.03 (–18.51) | S (S) |
| | Validation | 0.71 (0.45) | 0.54 (0.74) | 0.90 (0.83) | –6.69 (–15.07) | G (US) |
| Saistaganj (5) | Calibration | 0.43 (0.34) | 0.76 (0.81) | 0.60 (0.39) | –37.88 (–34.83) | US (US) |
| | Validation | 0.05 (–0.43) | 0.98 (1.20) | 0.43 (0.17) | 17.84 (28.62) | US (US) |
| Sylhet (13) | Calibration | 0.85 (0.79) | 0.39 (0.45) | 0.89 (0.84) | –11.03 (–12.30) | G (G) |
| | Validation | 0.90 (0.79) | 0.31 (0.46) | 0.90 (0.79) | 1.91 (0.22) | VG (VG) |
| Bhairab (15) | Calibration | 0.70 (0.61) | 0.55 (0.63) | 0.83 (0.76) | 15.97 (17.06) | S (S) |
| | Validation | 0.14 (0.21) | 0.93 (0.89) | 0.71 (0.78) | 5.85 (17.39) | US (US) |

| | | | | |
|---|---|---|---|---|
| Very good (VG) | $0.75 < NSE \le 1.00$ | $0.00 < RSR \le 0.50$ | PBIAS $< \pm 10$ | |
| Good (G) | $0.65 < NSE \le 0.75$ | $0.50 < RSR \le 0.60$ | $\pm 10 \le$ PBIAS $< \pm 15$ | |
| Satisfactory (S) | $0.50 < NSE \le 0.65$ | $0.60 < RSR \le 0.70$ | $\pm 15 \le$ PBIAS $< \pm 25$ | |
| Unsatisfactory (US) | $NSE \le 0.50$ | $RSR > 0.70$ | PBIAS $\ge \pm 25$ | |

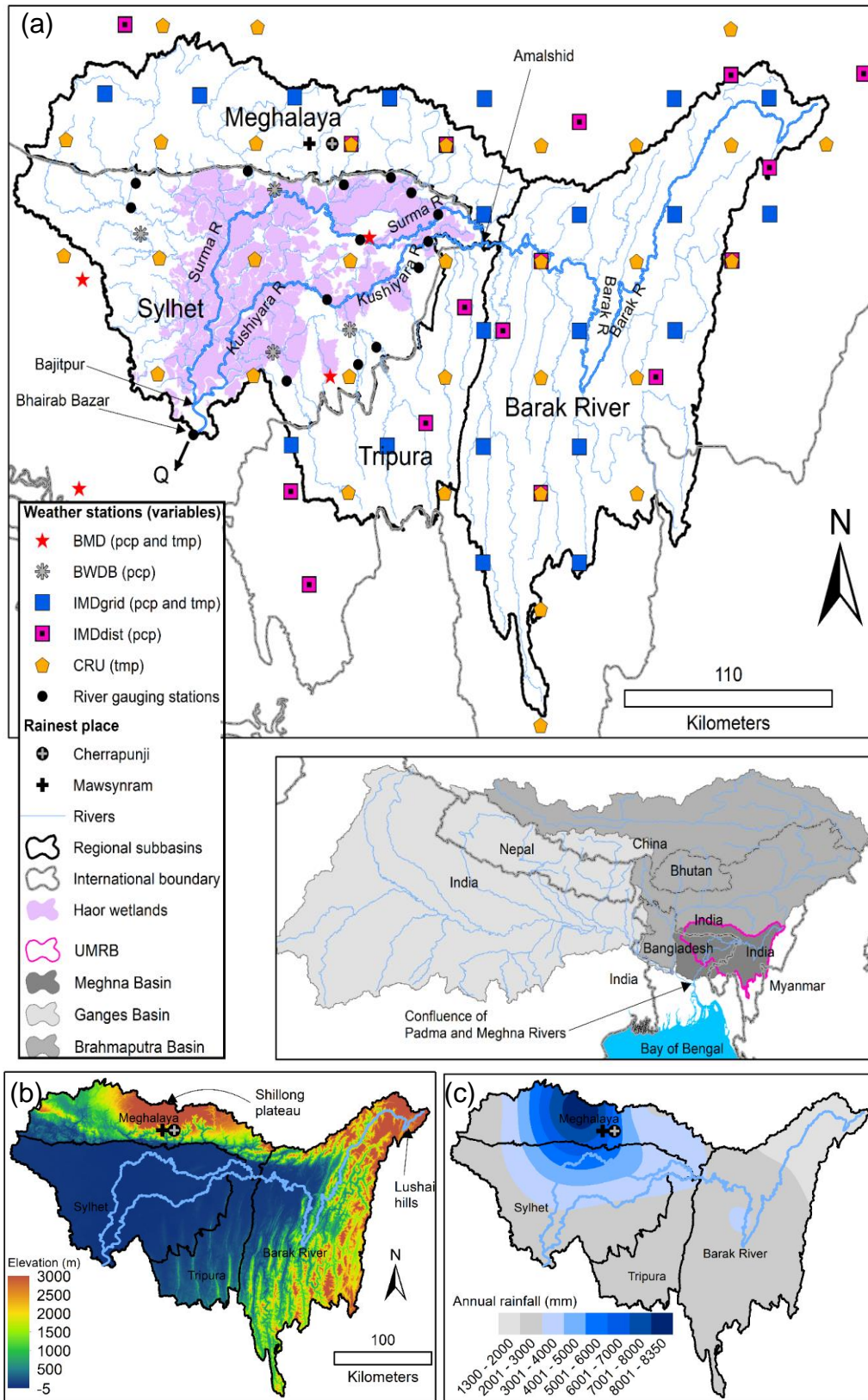[a]Simulation performance is graded based on the framework suggested by Moriasi et al. (2007).

**Figure 1.** (a) The Upper Meghna River Basin (UMRB). (b) Elevation map derived from Shuttle Radar Topography Mission (SRTM) data (see Table 1). (c) Rainfall map prepared by spatially interpolating (ordinary kriging) mean annual (1990–2003) rainfall from 28 meteorological stations (BMD, BWDB and IMDgrid). BMD: Bangladesh Meteorological Department; BWDB: Bangladesh Water Development Board, IMDgrid: gridded data of the Indian Meteorological Department (IMD); IMDdist: district average data of the IMD; CRU: Climatic Research Unit, University of East Anglia, UK; pcp: precipitation; and tmp: temperature.

Step 1: Catchment discretization into homogeneous climate zones (HCZ)
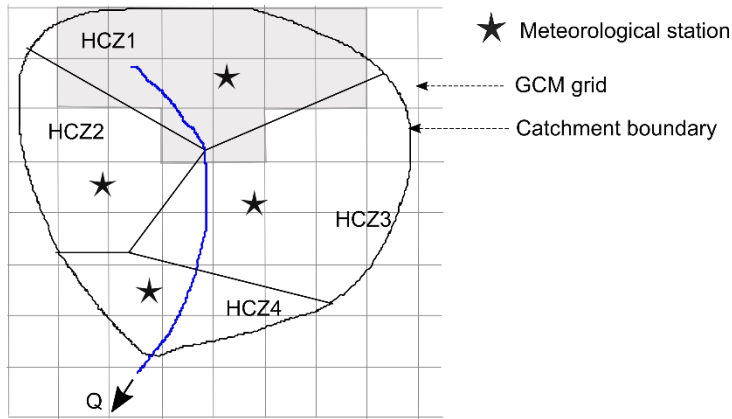


Step 2: Spatial averaging of time series data of all GCM grids lying within a HCZ

| Obs. Rainfall within a HCZ | Raw GCM rainfall at each grid lying within a HCZ | | | | | Averaged GCM rainfall |
|---|---|---|---|---|---|---|
| | Grid_1 | Grid_2 | Grid_3 | ………… | Grid_n | |
| 0 | 2 | 0 | 1 | ………… | 0 | 2 |
| 5 | 10 | 3 | 6 | ………… | 3 | 8 |
| 10 | 5 | 7 | 13 | ………… | 7 | 14 |
| 2 | 15 | 6 | 8 | ………… | 0 | 5 |
| . | . | . | . | ………… | . | . |
| . | . | . | . | ………… | . | . |
| . | . | . | . | ………… | . | . |

Step 3: Clustering data (obs. and GCM) under each calendar month

| Rainfall data grouped under each calendar month | | | | | | | | |
|---|---|---|---|---|---|---|---|---|
| January | | February | | March | | ………… | December | |
| Obs. | GCM | Obs. | GCM | Obs. | GCM | ………… | Obs. | GCM |
| 0 | 1 | 3 | 0 | 10 | 5 | ………… | 0 | 1 |
| 1 | 2 | 8 | 6 | 15 | 35 | ………… | 0 | 0 |
| 0 | 0 | 5 | 3 | 50 | 22 | ………… | 3 | 2 |
| . | . | . | . | . | . | ………… | . | . |
| . | . | . | . | . | . | ………… | . | . |
| . | . | . | . | . | . | ………… | . | . |

Step 4 & 5: Construction of CDF curves (obs. and GCM) and estimation of biases
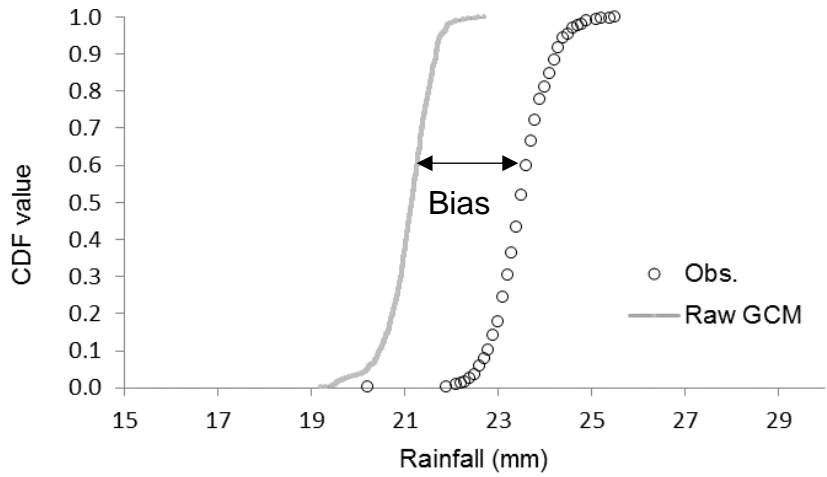


**Figure 2.** The five sequential steps of the quantile mapping bias-correction method.
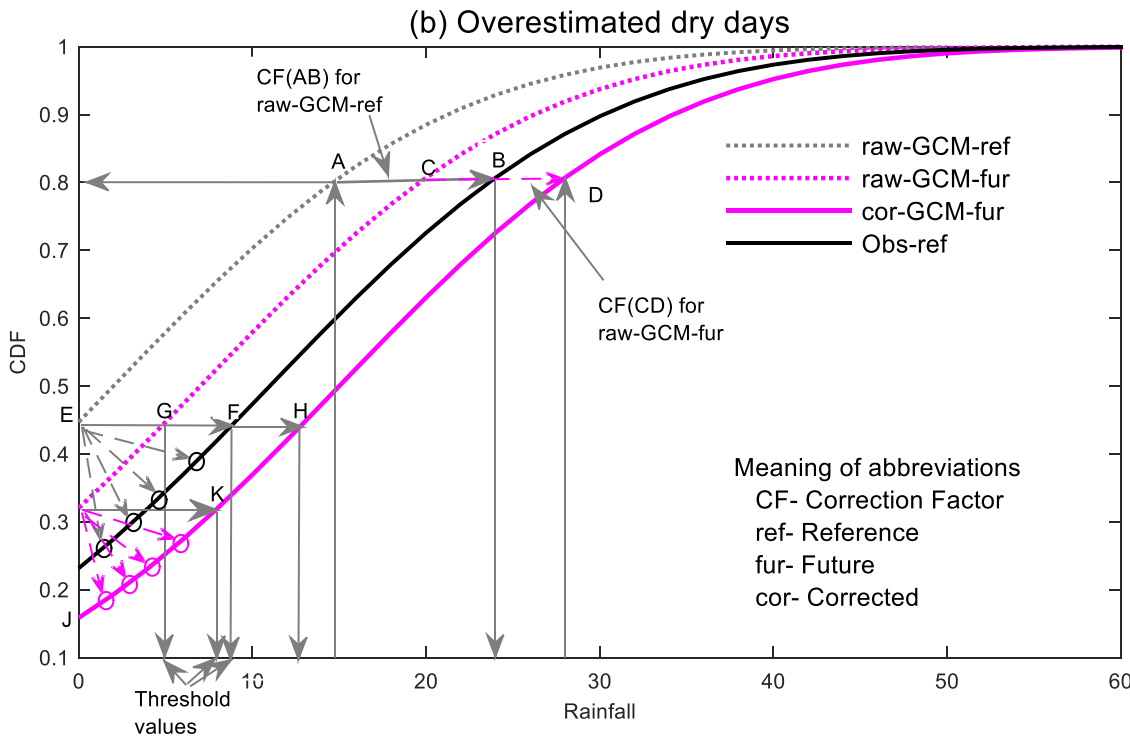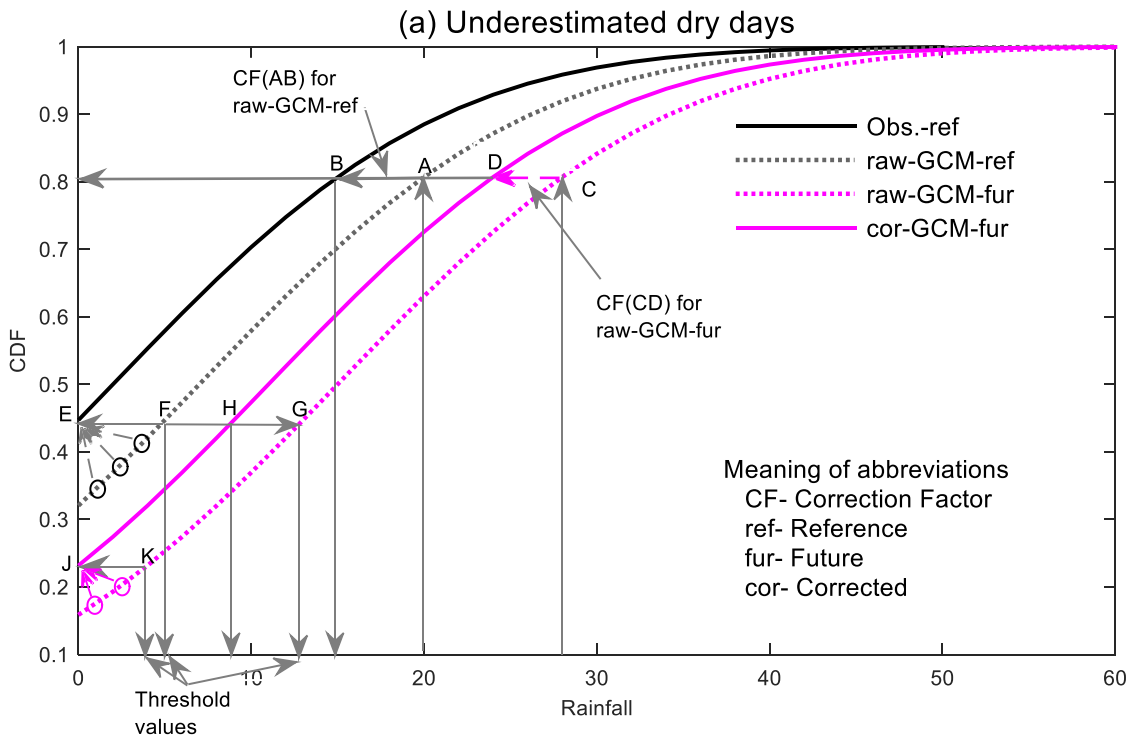
**Figure 3.** Graphical representation of the quantile mapping (QM) bias-correction method. The value of cumulative probability density or cdf at 0 rainfall indicates the dry day frequency of each curve i.e. the percentage of dry days in the respective time series.
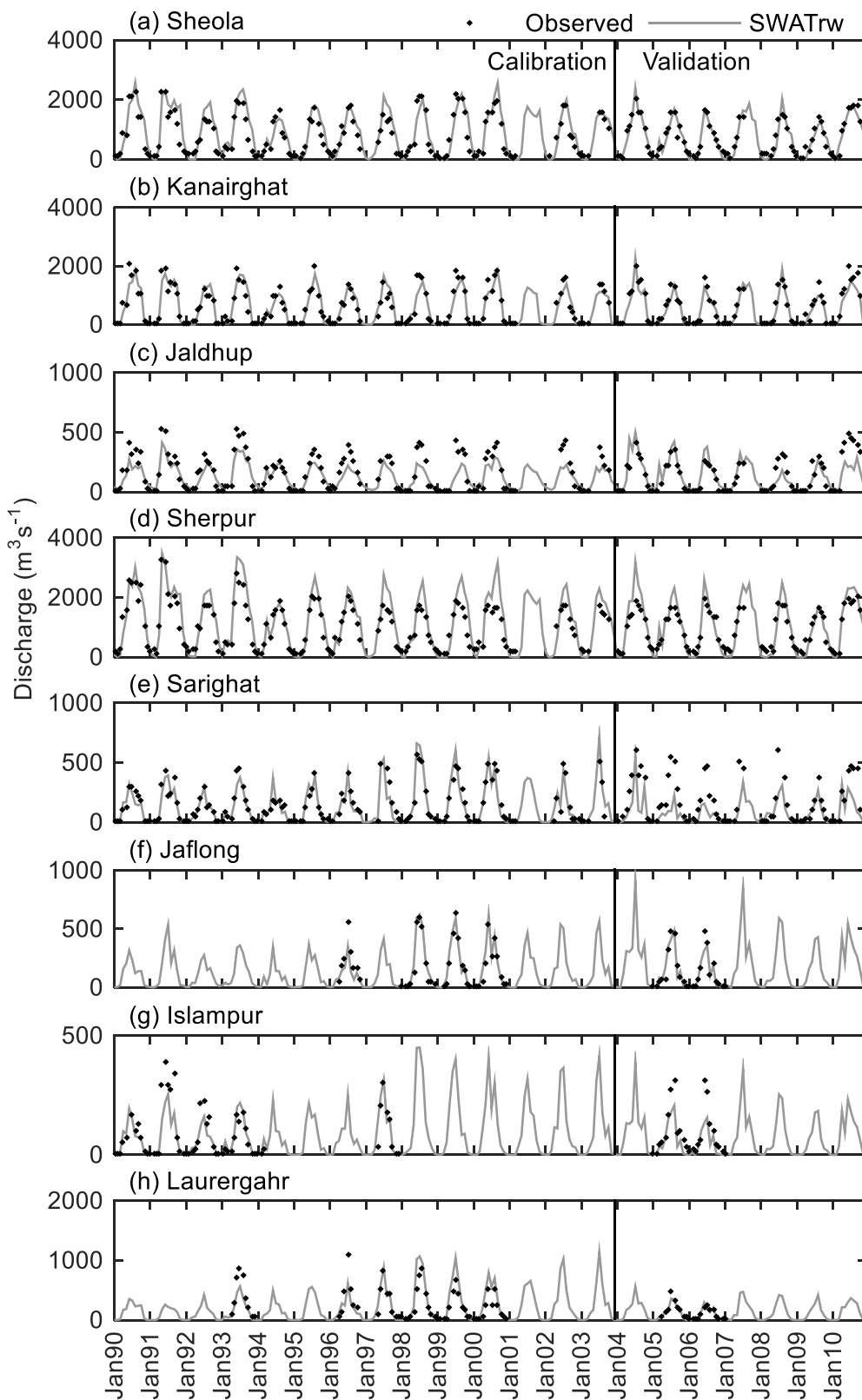
**Figure 4.** Observed and SWATrw-simulated mean monthly discharge at eight river gauging stations in the UMRB. Calibration (1990–2003) and validation (2004–2010) periods are indicated (note different y-axis ranges).
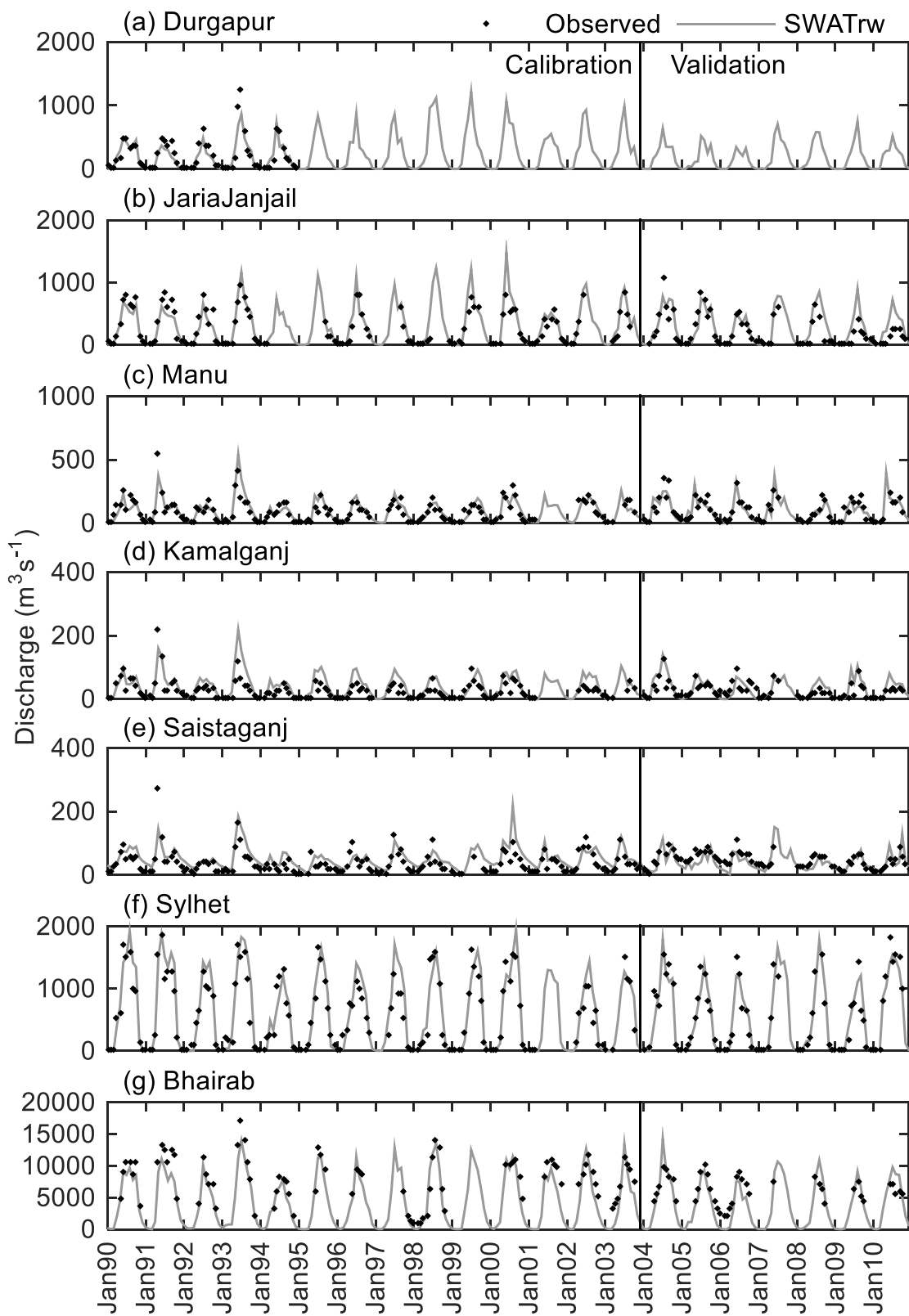
**Figure 5.** Observed and SWATrw simulated mean monthly discharge at seven river gauging stations in the UMRB.

Calibration (1990–2003) and validation (2004–2010) periods are indicated (note different *y*-axis ranges).
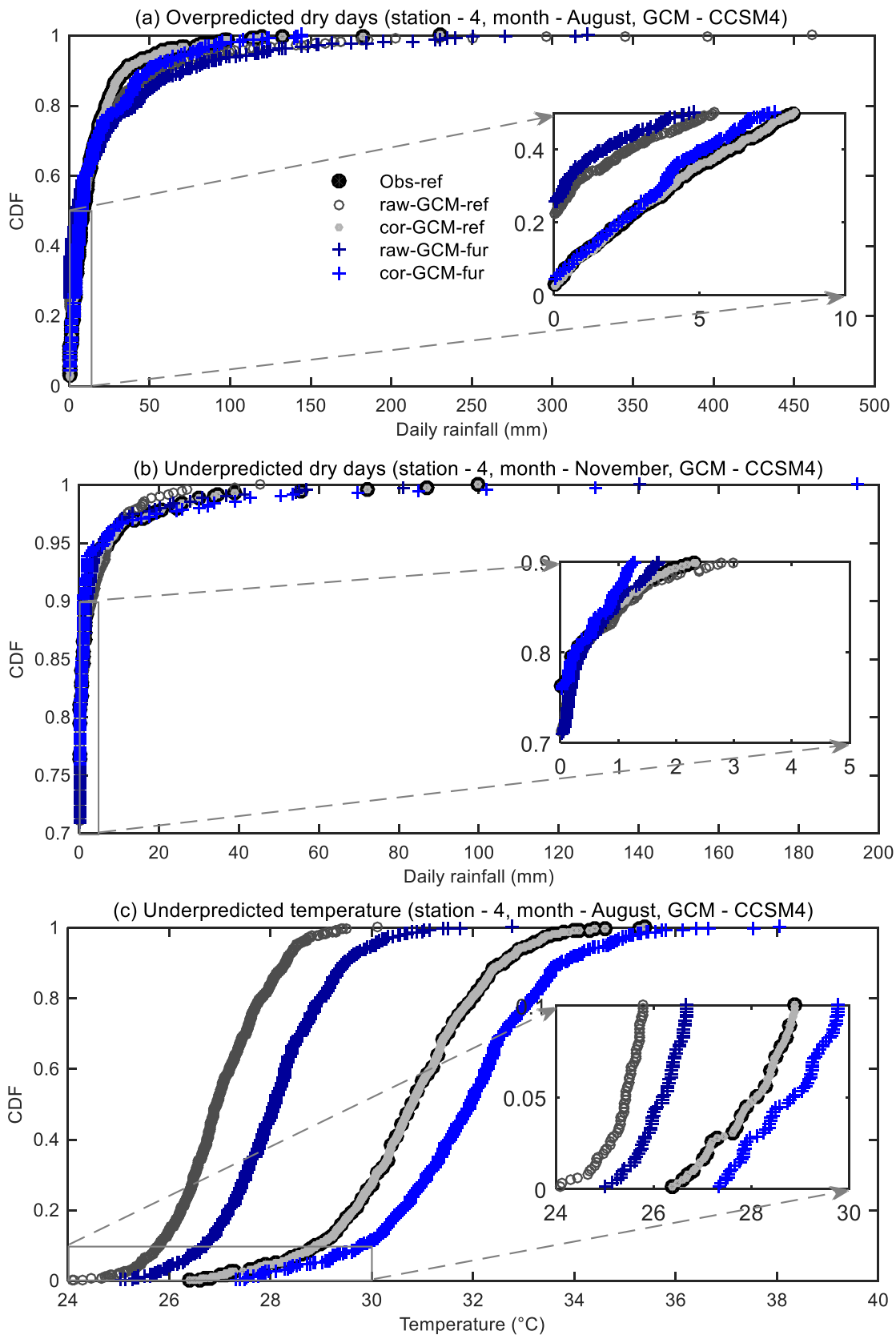
**Figure 6.** Comparison of raw and QM bias corrected daily rainfall per calendar month: (a) over-predicted and (b) under-predicted dry days (or cdf) in the reference period (1981–2000); and (c) temperature for one calendar month (August). The inset in each subplot is a magnification of the lower left part of the respective figure.
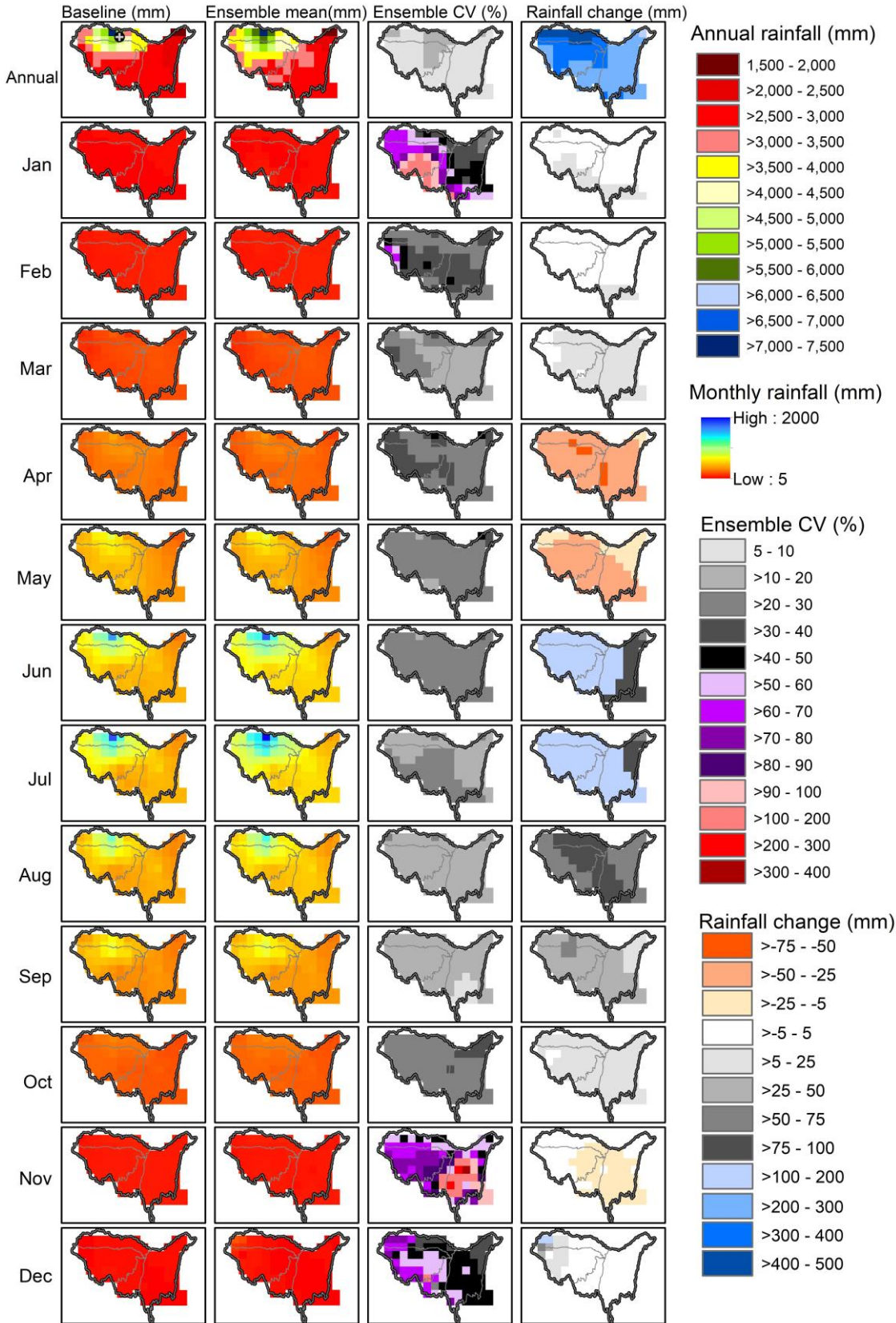
**Figure 7.** Comparative demonstration of baseline (1981–2000) and bias-corrected projected (2031–2050) rainfall over the UMRB. From left to right: projected mean (annual and monthly) rainfall derived from the ensemble of 17 GCMs; coefficient of variation (CV) in rainfall projections across the 17 GCMs; and summary of the projected change in rainfall totals (annual and monthly) compared to the baseline. The deterministic IDW spatial interpolation method was used to derive the gridded maps from rainfall (baseline and projections) at the 26 meteorological stations.
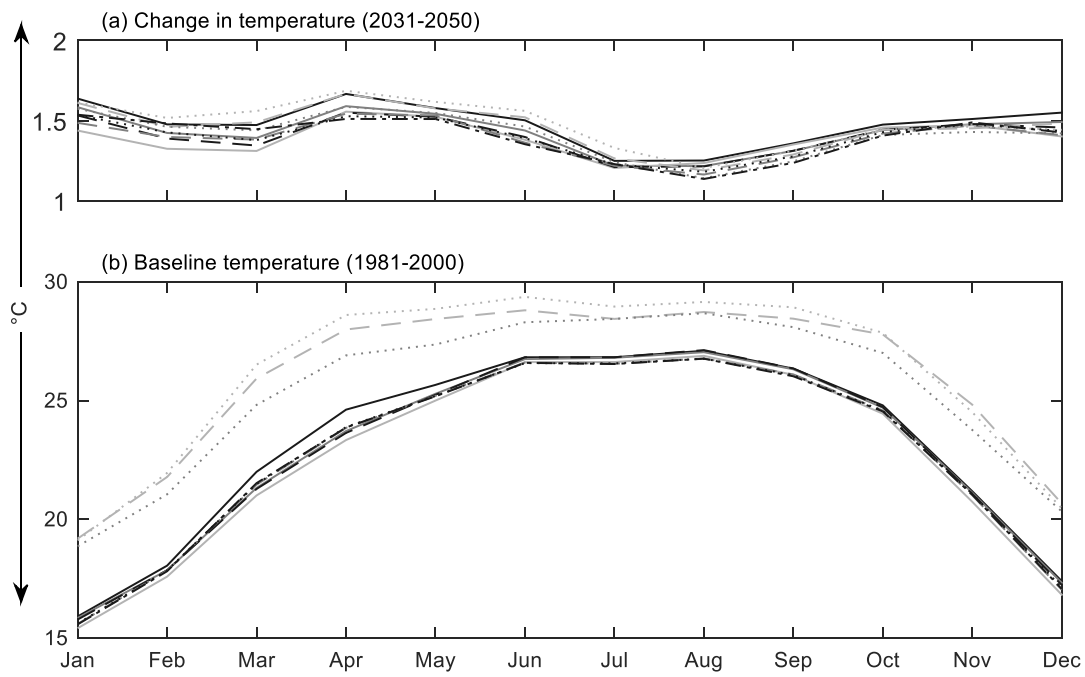
**Figure 8.** (a) Changes in bias-corrected ensemble mean monthly temperature during the projected period (2031–2050) and (b) baseline mean monthly temperature at the 10 meteorological stations (each line represents an individual station).
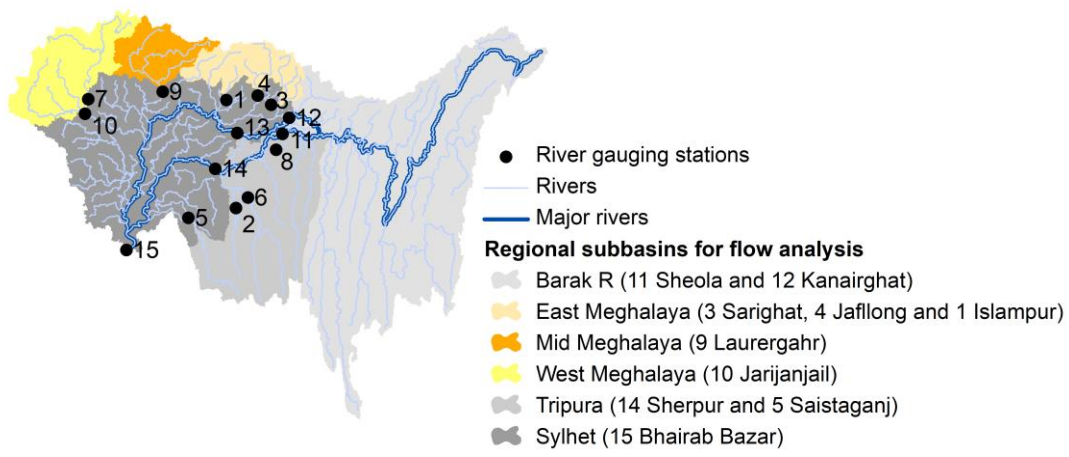
**Figure 9.** Six regional sub-basins of the UMRB used to analyse climate change impacts on river discharge.
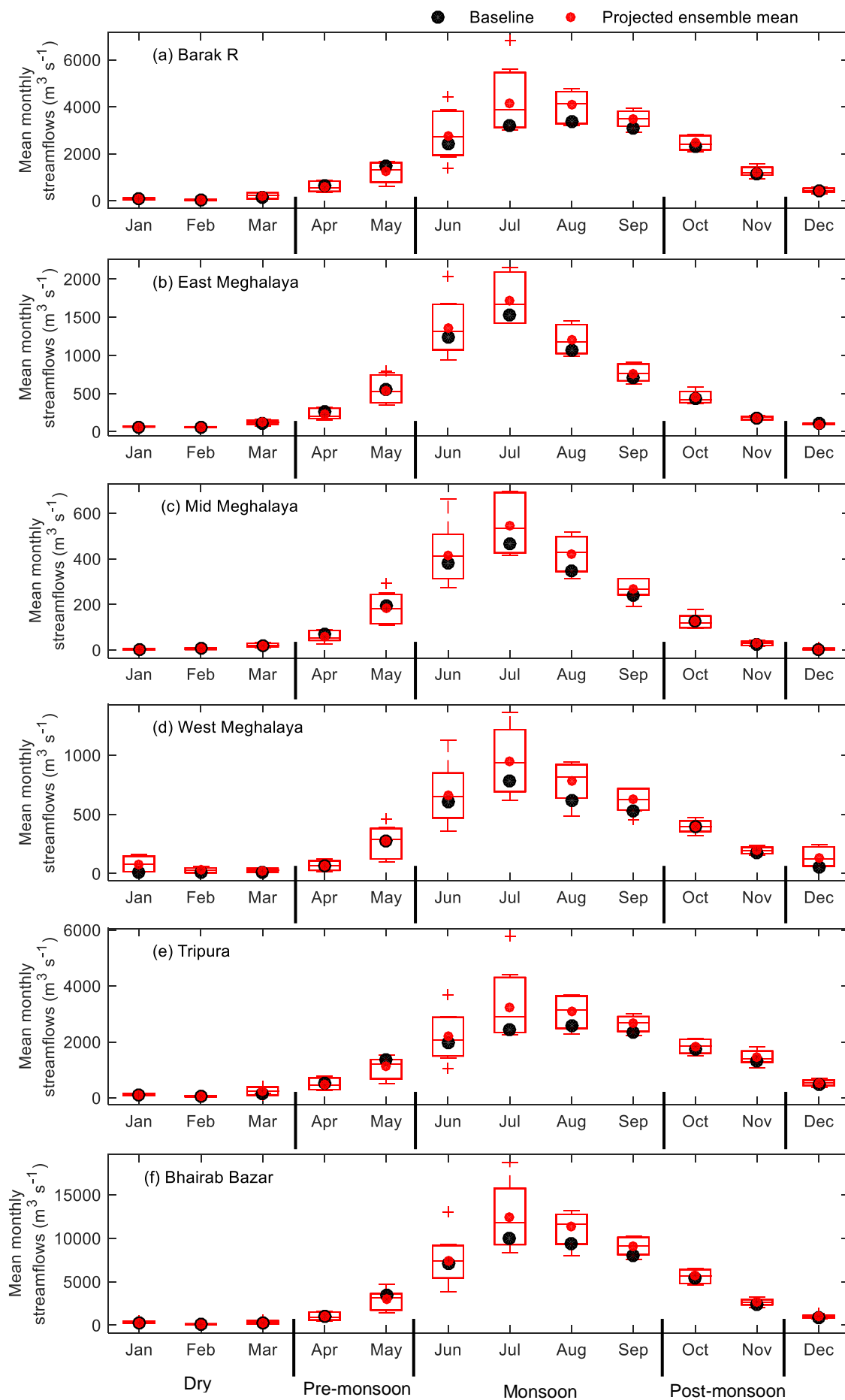
**Figure 10.** Baseline (1981–2000) and projected (2031–2050) mean monthly discharge at the outlet of major sub-basins within the UMRB. The box-and-whisker plots are generated using the mean monthly discharges projected by the 17 GCMs. The upper and lower limits of each box represent the 90th and 10th percentiles, respectively.
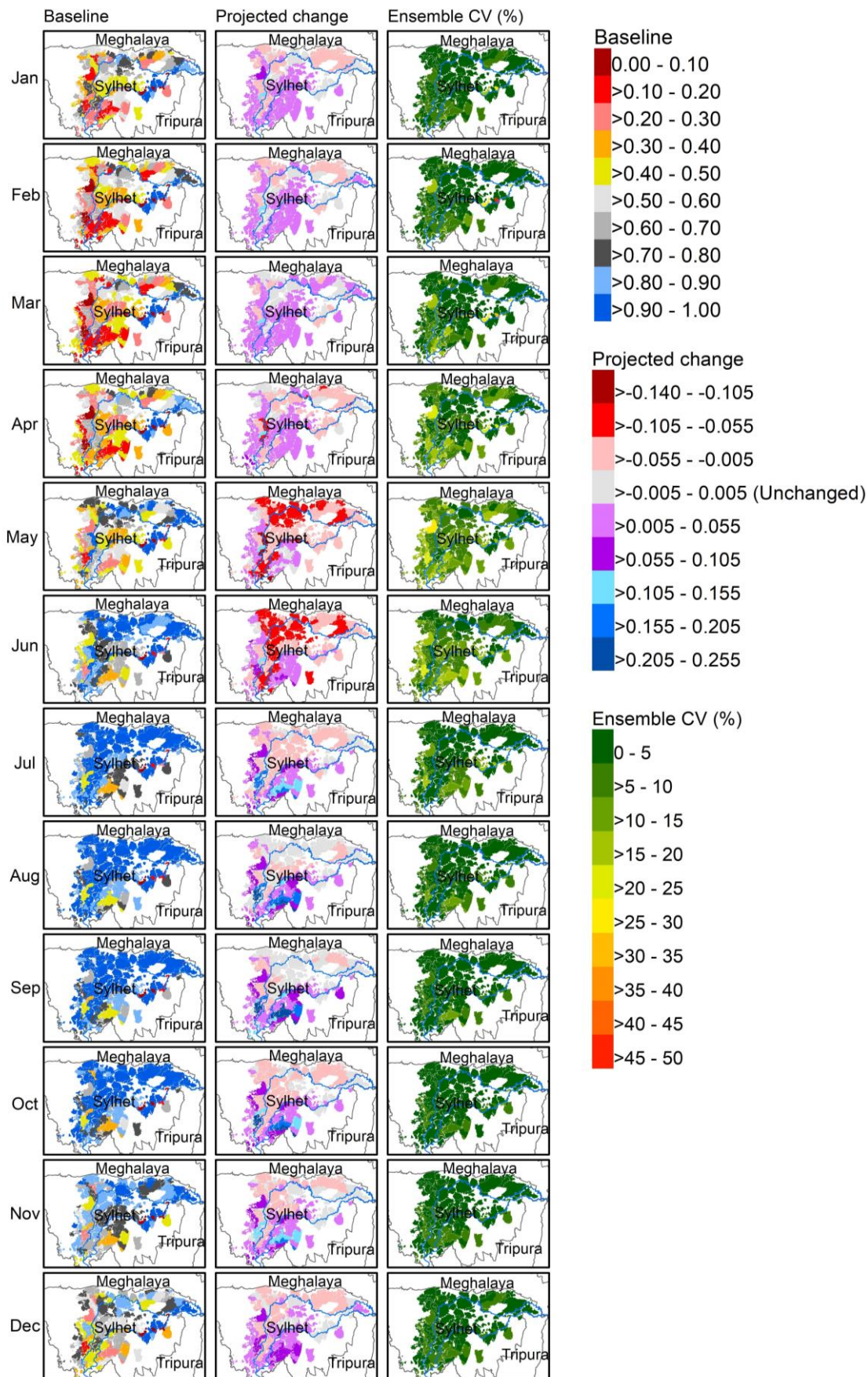
**Figure 11.** Mean monthly inundation fraction for each individual wetland in the lower UMRB (i.e. the Sylhet Basin) for (from left to right): the baseline period (1981–2000); projected changes from the baseline for the ensemble mean for 2031–2050; and CV across the 17 GCMs for 2031–2050.
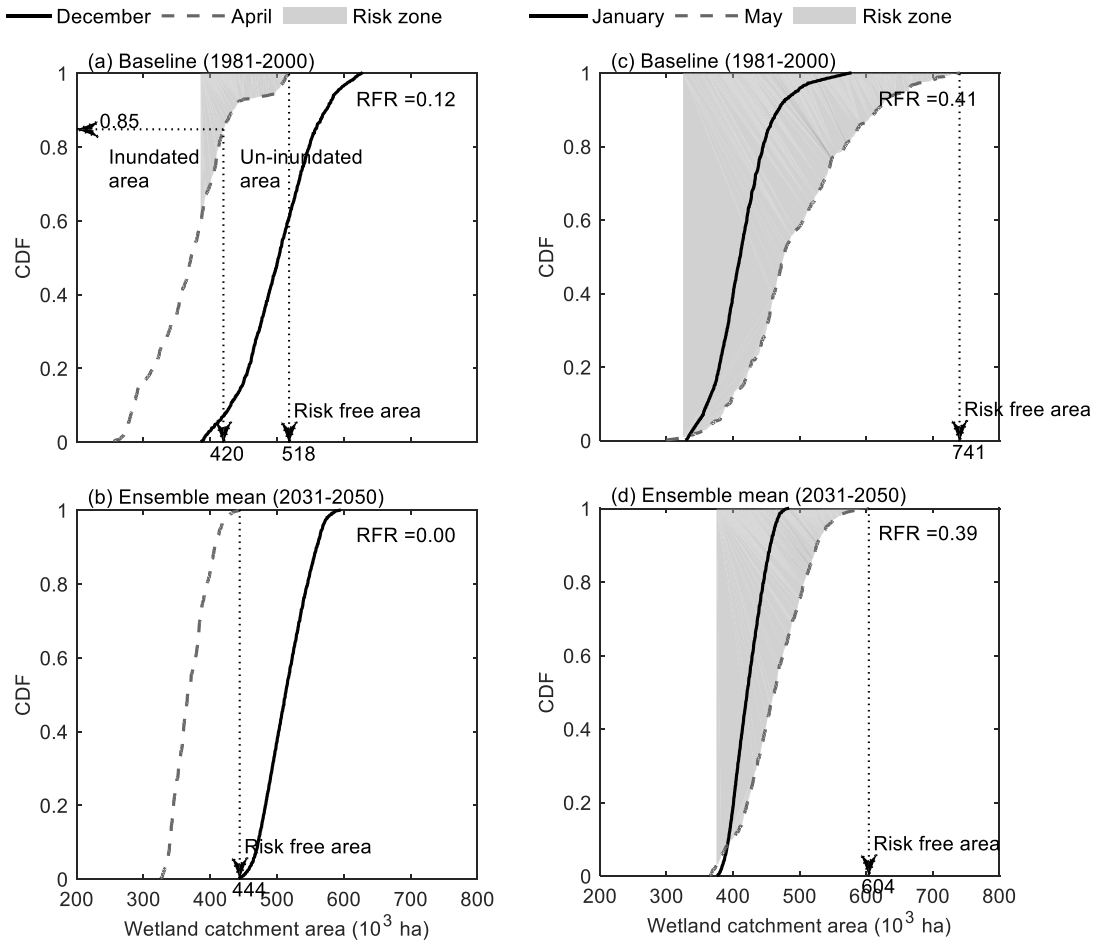
**Figure 12.** Estimated risk of Boro rice damage due to flash floods during harvest time for: (a) and (c) the baseline (1981–2000); and (b) and (d) ensemble mean for the future period (2031–2050). For (a) and (b), December and April are the planting and harvesting months, respectively, and for (c) and (d), these planting / harvesting periods are lagged by one month. A vertical line drawn through any point on a cdf curve demarcates the interface between inundated and un-inundated areas (see (a)). Any area beyond the highest inundation level during a harvesting month is denoted as flood-risk free for that month.

47

**Hydrological impacts of climate change on rice cultivated riparian wetlands in the Upper Meghna River Basin (Bangladesh and India)**

Mohammed M. Rahman [a,b,*], Julian R. Thompson [b], and Roger J. Flower [b]
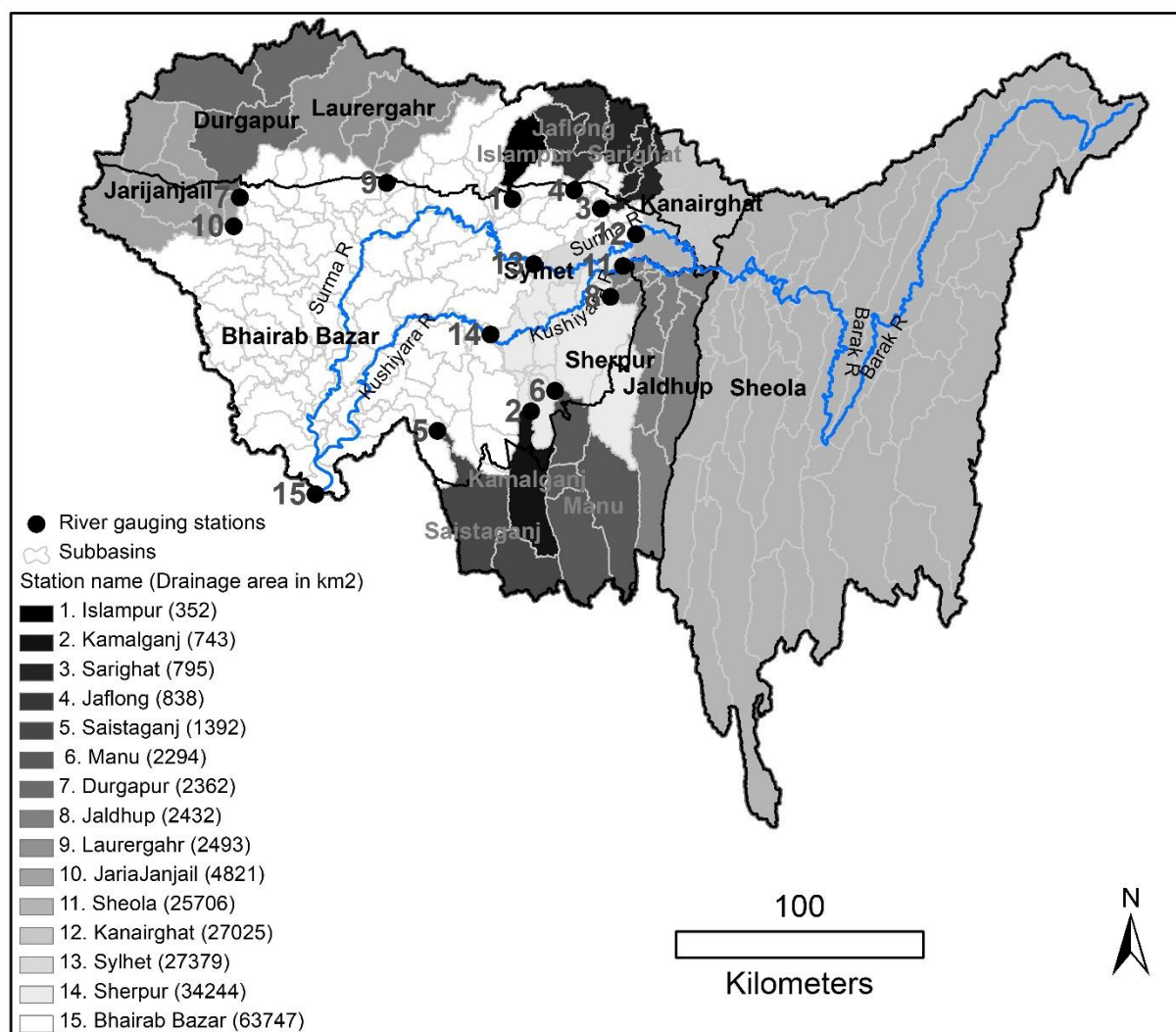


**Figure S1.** Delineated sub-basins within the UMRB and the total drainage area for each of the 15 gauging stations used in model calibration / validation.
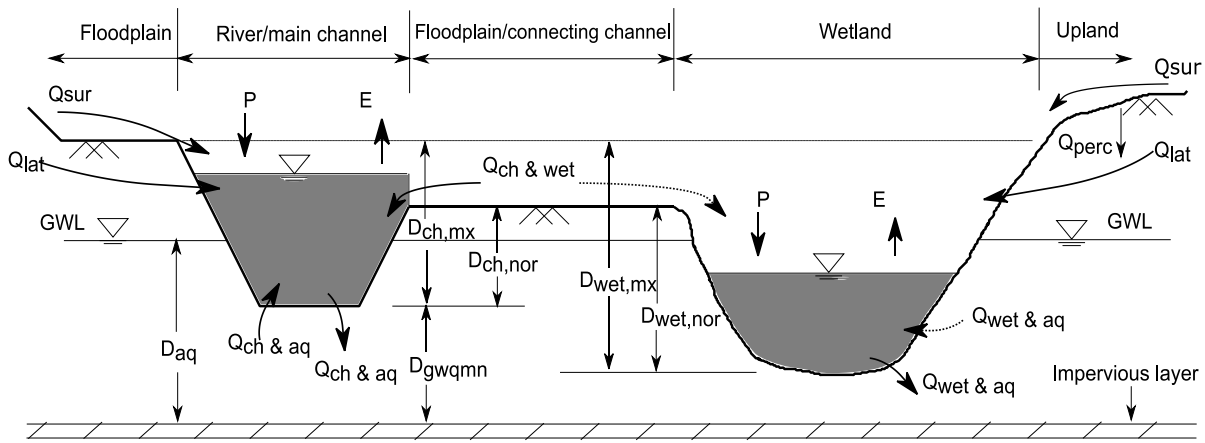
**Figure S2.** Hydrological interactions between a river, riparian wetland and aquifer in SWATrw. The extent of wetland shown with the double-headed horizontal arrow line is the extent at maximum wetland capacity. P= precipitation, E= evaporation, $Q_{perc}$ = percolation, $Q_{sur}$ = surface runoff, $Q_{lat}$ = lateral/inter flow, $Q_{ch\ \&\ aq}$ = exchange between river/main channel and aquifer, $Q_{ch\ \&\ wet}$ = exchange between the river/main channel and wetland, $Q_{wet\ \&\ aq}$ = exchange between the wetland and aquifer either over the floodplain or through the connecting channel, GWL = groundwater level, $D_{aq}$ = height of groundwater level above the aquifer's impervious layer, $D_{gwqmn}$ = height of river's bottom above the aquifer's impervious layer, $D_{ch,mx}$ = maximum channel depth, $D_{ch,nor}$ = channel depth from the normal level which is the elevation of river bank at connecting channel, $D_{wet,mx}$ = maximum wetland depth and $D_{wet,nor}$ = normal depth of wetland. Processes drawn with the dotted lines ($Q_{ch\ \&\ wet}$ and $Q_{wet\ \&\ aq}$) are not currently modelled in SWAT but are included in SWATrw (Rahman et al., 2016).
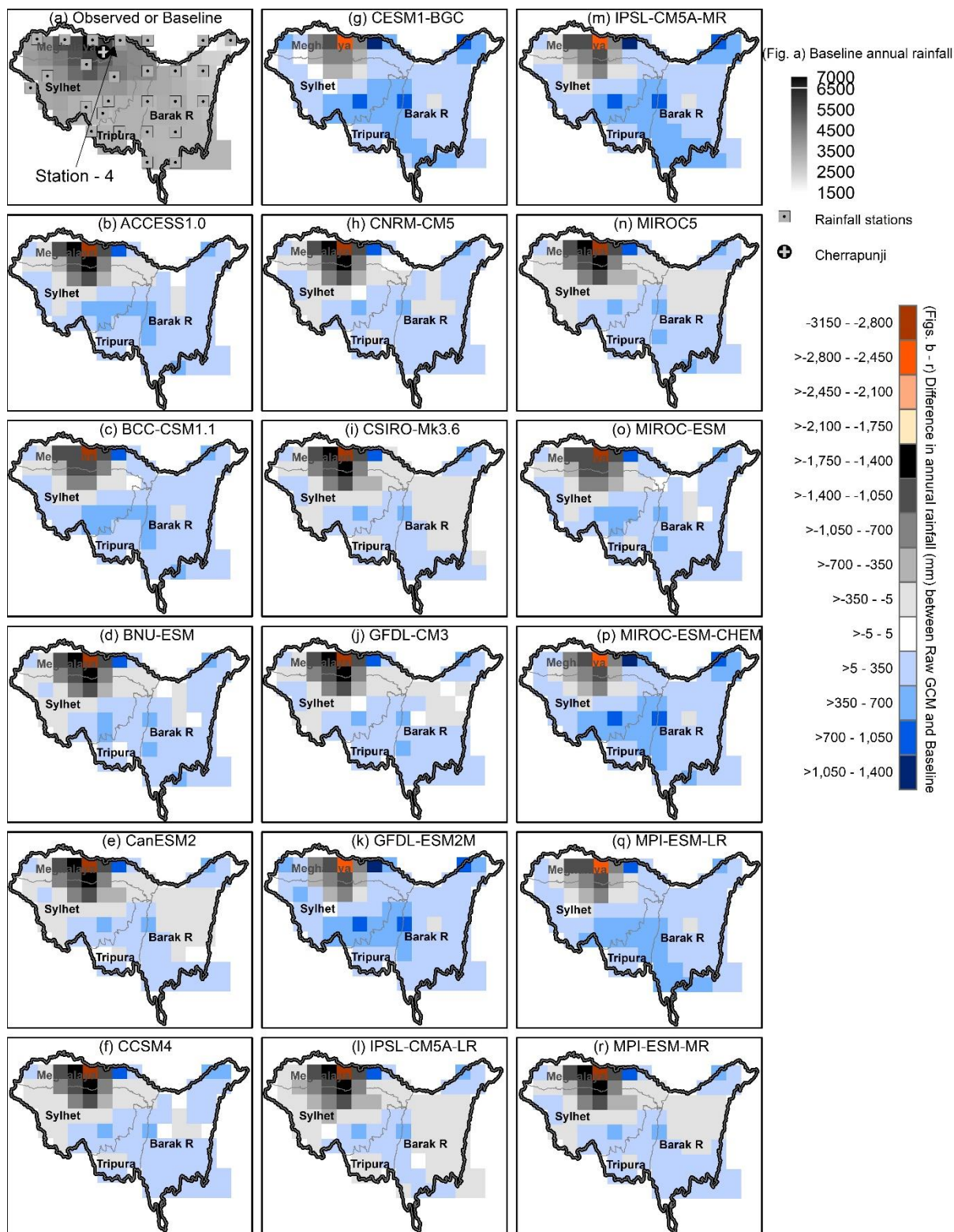
**Figure S3.** Anomalies between raw GCM data (NEX-GDDP) and observed mean annual rainfall for the baseline period (1981–2000). Subplots (b)–(r) are derived by subtracting gridded observed mean annual rainfall from the corresponding value of respective raw GCMs. The deterministic Inverse Distance Weighted (IDW) spatial interpolation method was used to produce the gridded maps from mean annual rainfall at the 26 meteorological stations in the UMRB.
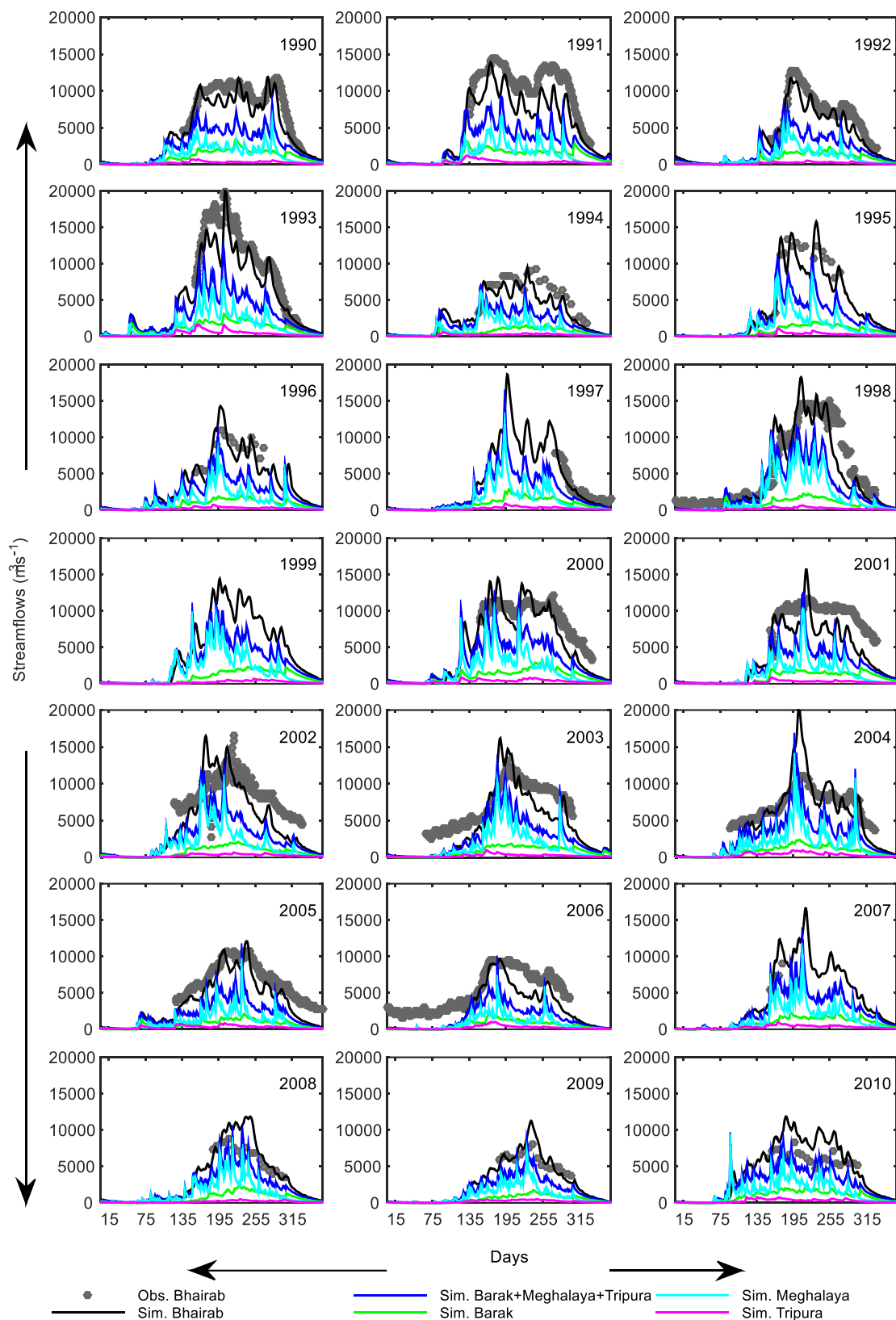
**Figure S4.** Comparison of daily discharges at Bhairab (the outlet of the UMRB) on the Meghna River with those from three large upstream catchments; Barak, Meghalaya and Tripura (see Fig. 1). For each of the last two catchments, daily discharge is calculated by summing simulated daily outflows of all transboundary rivers entering the lower Sylhet catchment in Bangladesh. Similarly, the total hydrograph of the three upper catchments is derived by summing their individual hydrograph ordinates for a particular day. The difference between the hydrographs of the UMRB and the combined three large upstream catchments is the potential runoff generated from the lower Sylhet catchment.
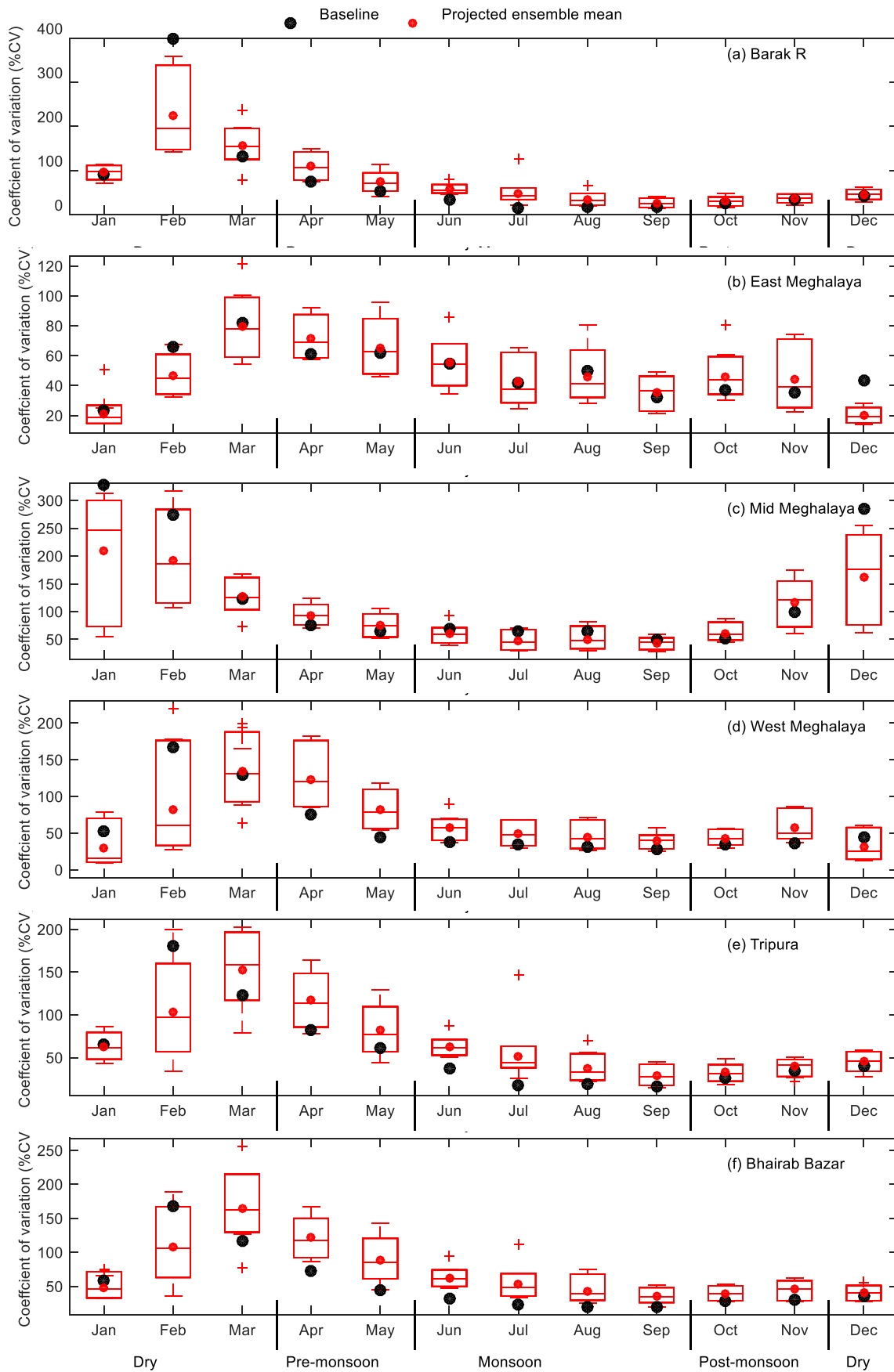
**Figure S5.** Baseline (1981–2000) and projected (2031–2050) coefficient of variation (CV) of mean monthly discharge at the outlet of major sub-basins within the UMRB. The box-whisker plots are generated using the mean monthly discharges projected by the 17 GCMs. The upper and lower limits of each box represent the 90th and 10th percentiles.
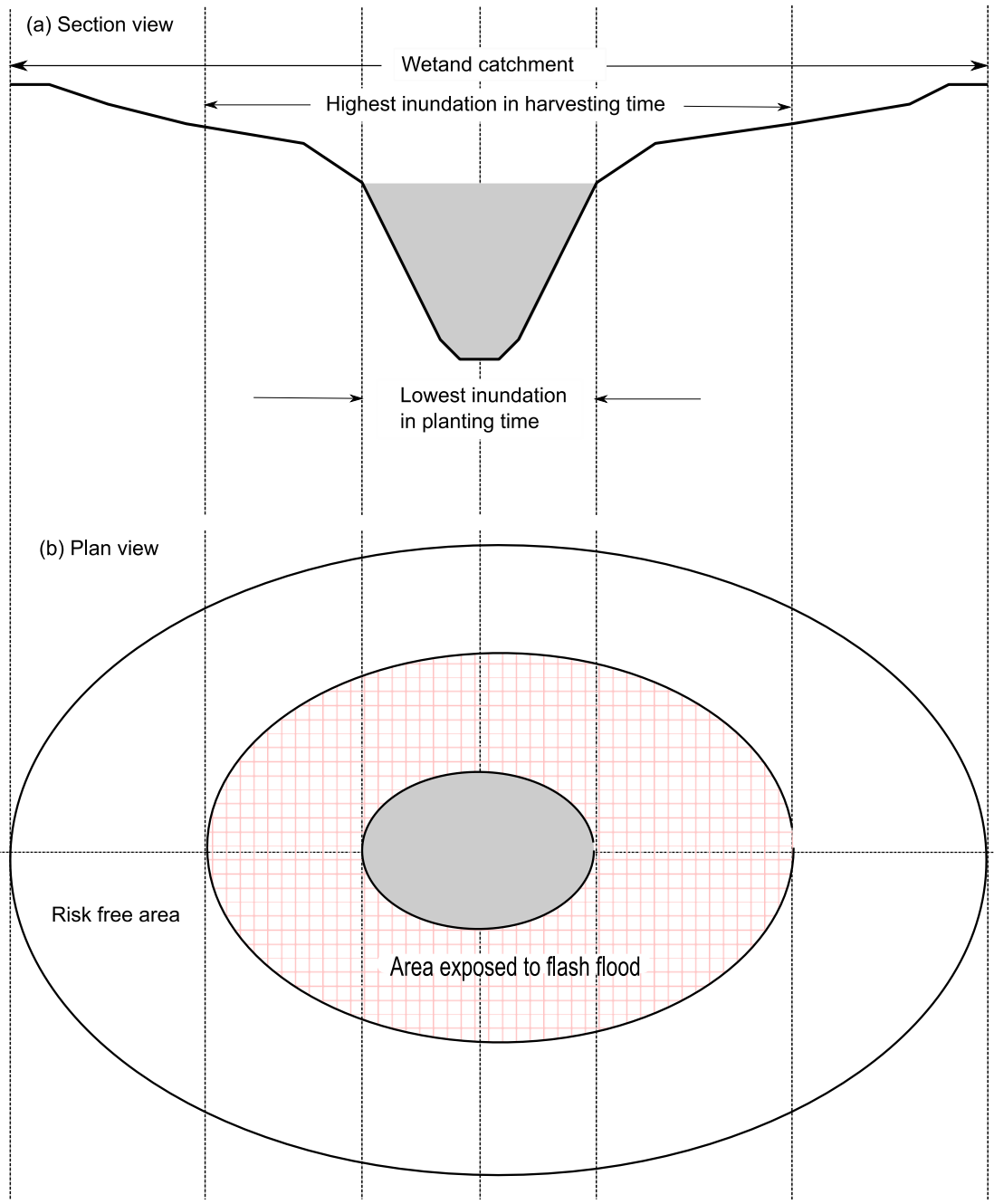
52

**Figure S6.** Potential wetland area exposed to flash flooding during harvesting time with respect to planting time. Any area above the highest inundation level is flood-risk free during harvesting time.